공학박사학위논문

Hazardous Chemical Dispersion Analysis and Surrogate Model Optimization using Artificial Neural Network

유해화학물질 확산 분석 및 인공신경망을 사용한 대리 모델 최적화

2017년 8월

서울대학교 대학원

화학생물공학부

양 시 엽

Abstract

Hazardous Chemical Dispersion Analysis and Surrogate Model Optimization using Artificial Neural Network

Seeyub Yang

School of Chemical & Biological Engineering

The Graduate School of Seoul National University

CFD simulations can be used to estimate the accident consequences by hazardous chemical releases. Both strength and weakness of this method lies on the complexity of the CFD simulation. In other words, CFD can predict chemical dispersion in the complex geometry like urban area, but it takes much computational resources.

Comparison between actual dispersion and CFD simulation is done to show usefulness of the CFD simulation. Anhydrous hydrogen fluoride dispersion field test is simulated and it is within the dispersion model criteria. Actual

hydrogen fluoride accidental release in 2012 is also simulated and its human and environmental damage prediction is similar to actual accident consequences.

Case study of the toxic gas dispersion in the urban area varying source and meteorological condition is conducted, and numerical method is tested for the worst case scenario. Time variant CFL stepping method and multi-threading reduce the calculation time. Also ANN is able to classify the safe and danger based on the input condition.

CFD simulation can be applied in the detector allocation problem in the process unit. Simulation inputs are determined by computer experiment procedure and other sets of data detection time is estimated with ANN. Then based on these simulated and estimated data MILP is solved and showed better result than using simulation data alone.

Keywords: Computational Fluid Dynamics; Chemical Safety; Artificial Neural Network; Mixed Integer Linear Programming; Surrogate Model
Student ID: 2011-21045

Contents

List of Figures

List of Tables

CHAPTER 1 : Introduction

1.1. Research motivation

Prediction of chemical accident consequences is one of the key interests in the process systems industries. Among many calculation methods that can predict the loss generated by the hazardous chemicals, computational fluid dynamics (CFD) is a method that gathers attention. Thanks to enhancement of computational power, CFD can now be considered as a feasible option when calculating damage to human and environment by chemical accidents such as explosion, fire and toxic release. CFD can be used for simulate discharge, dispersion and explosion of chemical materials. In the field of dispersion calculation, many researchers adjusted their one or two dimensional models to simulate the effect of slopes and ramps, fences and vapor barriers, buildings and complex terrains. Still, three-dimensional fluid dynamic model has shown its strength in the situation of complex geometries.

Despite of its good accuracy in a general and complex geometry, a CFD model needs a lot of computational resources. And that is preventing this model to become the most popular model in the process safety field. The number of simulation result should be limited and one cannot use the CFD model to conduct extensive sensitivity tests considering available computing power is too often limited. So, some techniques in the computational experiment design can help build a model based on the CFD model that can reduce required simulation time.

This thesis deals with usefulness and methods to overcome drawbacks of CFD

model for dispersion of accidental chemical release.

1.2. Description of CFD model in this thesis

For CFD simulation in this entire thesis, FLACS version 10.4 which was released in 2015 is used. FLACS is a commercial CFD code having characteristics of a 3D Cartesian coordinate, finite volume method, k-ε turbulence model, RANS (Reynolds-averaged Navier-Stokes), and a first order backward Euler scheme. Mass, momentum, enthalpy, and mass fraction of species conservation equations are closed by the ideal gas law. Generally, the conservation equation can be shown like equation 1-1. And from first term to the last of the equation, they represent transient term, convection term, diffusion term, and source term, respectively. (Gexcon AS, 2015)

$$\frac{\partial}{\partial t}(\rho\phi) + \frac{\partial}{\partial x_j}(\rho u_i \phi) - \frac{\partial}{\partial x_j}\left(\rho \Gamma_\phi \frac{\partial}{\partial x_j}(\phi)\right) = S_\phi \qquad \text{(Eq. 1-1)}$$

Where,

t: time

ρ: density

Φ: time dependent physical property

x_j: Cartesian coordinate (jth direction)

u_i: convective velocity in ith direction

Γ_Φ: diffusive property of Φ

S_Φ: source term of Φ

1.3. Outline of the thesis

The thesis is organized as follows. Chapter 1 provides general perspectives of the CFD modeling in the chemical dispersion. In chapter 2, CFD dispersion model is compared to a field test and an actual chemical release accident. In chapter 3, a case study of the CFD model in an urban area is done and attempts to reduce the model complexity is analyzed. In chapter 4, detector allocation optimization problem is solved as an application of CFD model in the process industries using mixed integer programming. Chapter 5 is a conclusion of the thesis.

Chapter 2: Comparison between CFD model and actual dispersion

2.1. Chapter outline

CFD model is known to be accurate than others. This chapter is to show the strength of the model. This chapter is composed of 2 main parts. First part 2.2 deals with validation study against field test. And latter part 2.3 deals with comparison study between CFD model and an actual chemical release accident. Large part of this chapter is based on the author's previous paper. (Seeyub Yang et al. (2017))

2.2. Validation of a CFD model against a field test

2.2.1 Validation objective

First of all, statistical performance measures were used based on the LNG vapor dispersion model evaluation protocol for validation purposes. (Ivings et al. 2012) The validation target was obtained using the maximum time-averaged concentration across an arc at a specified radius.

Mean Relative Bias (MRB):

$$\mathrm{MRB} = \left\langle \frac{C_m - C_p}{\frac{1}{2}(C_m + C_p)} \right\rangle \qquad \text{(Eq. 2-1)}$$

Mean Relative Square Error (MRSE):

$$\text{MRSE} = \left\langle \frac{(C_m - C_p)^2}{\frac{1}{4}(C_m + C_p)^2} \right\rangle \qquad \text{(Eq. 2-2)}$$

Where, C_m is Measured Concentration, C_p is Predicted concentration, and <…> represents the average over all measured pairs of concentrations.

2.2.2. Validation results in literature

Olav R. Hansen et al. (2010) conducted validation of FLACS against experimental data sets of LNG vapor dispersion and concluded that FLACS can be considered as a suitable model for simulation of the dispersion of LNG vapor. (Hansen et al. 2010). And various other gases (Hanna et al. 2004). Furthermore, an anhydrous ammonia field test was validated with Desert Tortoise data (Ichard. 2012). However, the Goldfish test, an anhydrous hydrogen fluoride field test has not yet been reported.

2.2.3. The Goldfish hydrogen fluoride spill field test

The purpose of this field test validation is to find appropriate settings that can be applied to actual accidental cases and eventually to universal CFD calculations for any hypothetical scenario. Thus, high computational loads should be avoided; instead light, still valid model parameters are essential. A relatively rough grid of 10 m × 10 m × 3 m was used for a single-phase approach.

There are 3 sets of field tests for validation, namely GF1, GF2, and GF3. Data from GF4-6 was tested with a water curtain and it is not of interest for the purposes of this validation study. The result can be found in the field test report (Blewitt et al. 1987). Table 1 shows basic test input information.

For the dispersion result calculation, the single gas-phase leak and liquid-vapor leak were calculated. Single-phase dispersion calculation can run in parallel to a multi-core process. The Homogeneous Equilibrium Model (HEM) is a simpler modeling approach when it comes to two-phase chemical dispersion, which assumes local thermal and kinematic equilibrium. However, it cannot be computed in parallel with a FLACS engine.

.

Table 1 Goldfish anhydrous hydrogen fluoride gas leak experiment test information

	UNIT	GF1	GF2	GF3
DATE		01-Aug-86	14-Aug-86	20-Aug-86
SPILL RATE	m^3/min	1.78	0.66	0.65
SPILL DURATION	min	125	360	360
WIND SPEED	m/s	5.6	4.2	5.4
TEMPERATURE	℃	37	36	26.5

2.2.4. Field test validation result

Before start of the dispersion model, discharge model should be made. In this study, simple Bernoulli equation based discharge model was tested. For the discharge model, measured volume discharge rate is 171.6 gal/min and predicted volume discharge rate is 168.8 gal / min. Deficiency between two is just 1.7%, which means that discharge rate can be calculated using Bernoulli equation.

$$\dot{m}(t) = C_d A\sqrt{2\rho_f(p(t) - p_a)} \quad \ldots \text{(Eq 2-3)}$$

Where,

$\dot{m}(t)$: mass flow rate ($\frac{\text{kg}}{\text{s}}$)

C_d: coefficient (0.62)

A: leak area (m^2)

ρ_f: density of fluid ($\frac{\text{kg}}{m^3}$)

p(t): pressure of the tank (Pa)

p_a: atmospheric pressure (Pa)

For the anhydrous ammonia field test, the Desert Tortoise was done in the same field in Nevada, USA. It was validated by Ichard's thesis (Ichard 2012). The concentration sensor was at 300 m, 1000 m, and 3,000 m; however the sensor at 3000 m did not catch the concentration peak of clouds in GF2. Like Ichard's thesis, only 300 m and 1000 m were tested. Table 2 shows the

validation result. Out of the six validation points, single-phase simulation provides all six, and two-phase simulation provides five points within the factor of two. There was not much difference between the single-phase and two-phase simulation results. Thus, the single-phase simulation is set as the base case scenario and used in the validation result comparison and in the modeling of the hydrogen fluoride gas leak. The mean relative error was 0.336 and mean relative square error was 0.134. Therefore, it satisfies the $-0.4<MRB<0.4$, and $MRSE<2.3$ criteria, meaning that the FLACS hydrogen fluoride dispersion model qualifies as a useful model (Ivings et al. 2013).

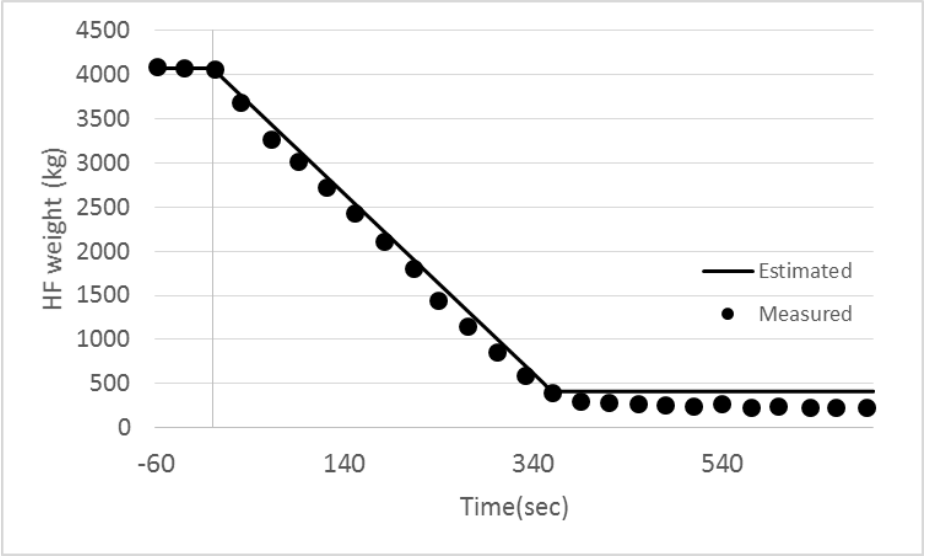

Figure 1 Measured result and estimated result of GF3 test HF time vs. remaining weight.

Table 2. Goldfish time averaged across an arc specified radius (Averaging time: 66.6 s).

	POSITION	OBSERVED	FLACS (SINGLE PHASE)	FLACS (TWO PHASE)
GF1	300m	25473	18628	15070
GF1	1000m	3098	2025	1895
GF2	300m	19396	13131	12120
GF2	1000m	2392	1326	1073
GF3	300m	18596	16565	15795
GF3	1000m	2492	2012	1662
		MRB	0.336	0.463
		MRSE	0.134	0.246

The validity of the Goldfish and Desert Tortoise models are proven by those found in Hanna et al. (1991). Figure 1 is the plot of mean relative bias (MRB) and mean relative square error (MRSE) for the result of two combined tests. FLACS has a MRB of 0.135 and MRSE of 0.068. It is near the origin, which means this CFD engine provides a good representation of the field test. The Britter and Mcquaid (B&M) model is the closest one among dispersions, but it is based on a set of simple equations and nomogram suggested in the 'Workbook on the Dispersion of Dense Gases', which fits curves to available field and laboratory data.

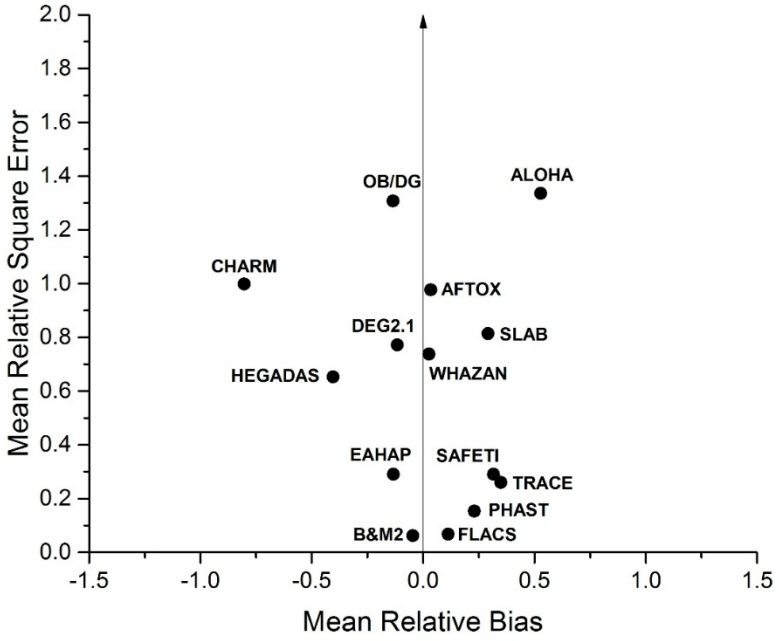

Figure 2 Goldfish and Desert Tortoise Validation results

2.3. Comparison between a CFD model and an actual accident

Toxic chemical leaks can cause severe damage to human beings and be disastrous for the environment. Studying past incidents is essential for understanding potential risks associated with toxic chemical leaks. This study uses computational fluid dynamics (CFD) to simulate the disastrous Gumi hydrogen fluoride gas leak of 2012 to compare simulated results with the actual damage it caused.

2.3.1. Accident description

This 2012 hydrogen fluoride gas leak brought forward the need for a national awareness around chemical safety to make systematic changes in laws, regulations, business cultures and accident responses of organizations on a national level for chemical safety management. (Lee et al. 2016) The ‘Chemicals Control Act’ passed legislation by the Korean Ministry of Environment and entered into force on January 1, 2015. With this new act, any person who intends to install and operate a hazardous chemical handling facility is required to prepare an evaluation in advance on how a chemical accident caused by hazardous substances would affect the environment external to the place of business. This, therefore, evaluates the impact of a chemical accident on people and the environment. (Chemical Controls Act, Section 2, Article 23).

The purpose of this part is to simulate the accident in Gumi and to compare it with the post-accidental data. To create realistic simulation settings, an

anhydrous hydrogen fluoride dispersion field test named Goldfish was tested before running CFD as a real case to define practical parameter sets.

The hydrogen fluoride accident occurred on September 27, 2012 at an LCD cleaning solvent production plant in Gumi, South Korea. The accident killed five people, injured 12, and damaged 2.4 km^2 of an agricultural field, in addition to causing harm to 3200 domestic animals (Korea Occupational Safety & Health Agency 2013). The leak's source was an 18-ton tank container, and CCTV footage from the scene showed a worker accidentally opening the lever. The accident occurred at 15:43 KST, and the valve was completely closed at 23:40. During the 8 hours for which the valve was open, between 8 and 12 tons of hydrogen fluoride gas were released (Lee et al. 2016; Joo 2013).

2.3.2. The hydrogen fluoride gas leak simulation setting

The prevailing wind at the time of the accident and on that day was blowing in the westerly direction, as shown in Figure 3. However, localized southerly or easterly winds could be observed. (Lee et al. 2013). Figure 3 shows data from the Automatic Weather Station recorded for the 2 hours following the accident. The Korean government announced the east side of the accident site as an especially damaged area.

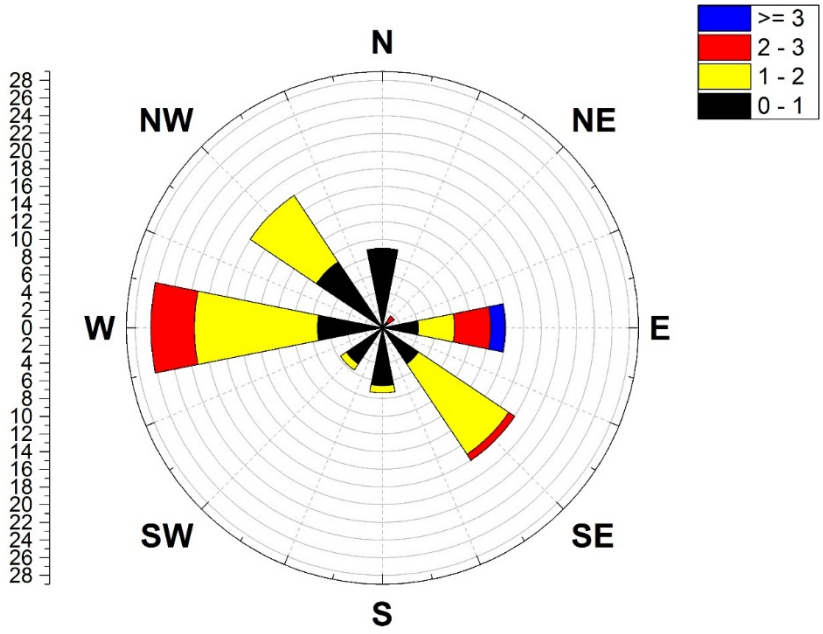

Figure 3 Wind rose recorded for 120 min after the accident, according to the nearest AWS station.

2.3.3. FLACS simulation settings

Geometric data around the accident site was provided by the National Spatial Information Clearinghouse of Korea and is shown in Figure 4. Instead of assuming a flat plane, the actual geometric characteristics were applied. The west wind encounters the hill in the east to change the local wind direction. By applying geometric contour lines provided from the CAD file, 25 m × 25 m rectangular parallelepiped shapes were created. The river across the south part of the simulation volume was ignored because it is out of the zone of interest. For the initial setting, previous simulation research data was used (Ko et al. 2015; Joo 2013; Yang et al. 2015) Each simulation is done with parallel computing using twelve CPU threads. The computer used in this research has 2.7 GHz/24 Core CPU and 256 GB DDR3 RAM.

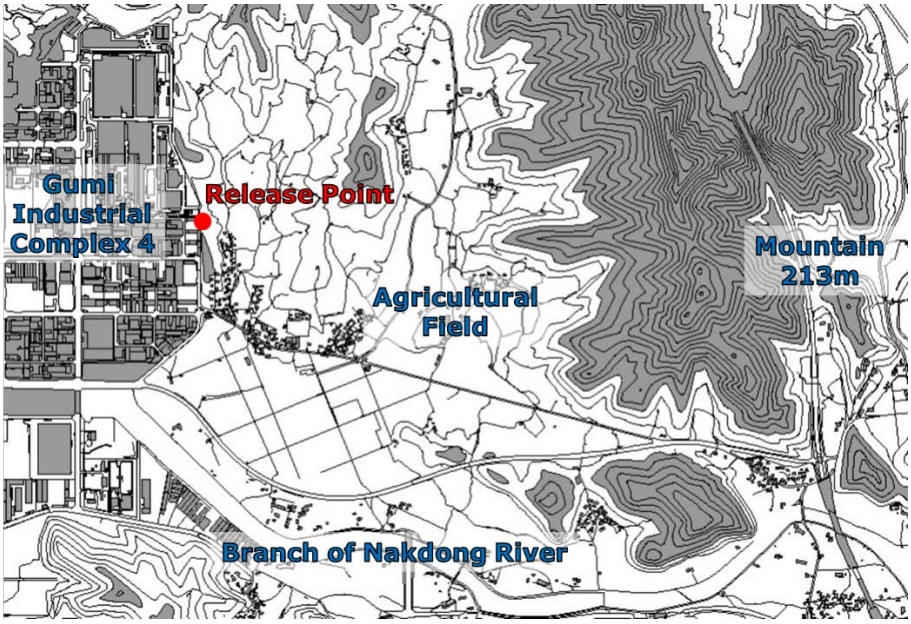

Figure 4 Geographic image of the accident site.

The simulation volume is 0.72 km^3, consisting of 2 km for the downwind direction, 1.8 km for the crosswind direction, and 0.2 km for the vertical direction. The simulation time was set to be 2 hours, which is enough time for all concentrations in the simulation volume to run under 1 ppm. The smallest grids, which are near the source, are 10 m × 10 m × 3 m as in the validation case, and become gradually larger by the factor of 1.2. The total number of defined control volumes is 330,750.

There is some uncertainty regarding the discharge rate. The maximum discharge duration is the approximate 8 hours it took to completely block the valve. One report used an NBC-RAMS model based on a 3-hour discharge duration because the ambient temperature was higher than the normal boiling point of hydrogen fluoride (Joo 2013). Another paper employed a LES model based on 30 minutes of the main discharge duration and an additional 18 minutes for the remaining discharge based on the chemical safety emergency response team blocking the source of the valve approximately 30 minutes after discharge begun. Based on the time-dependent tank pressure, 8 tons of gas are calculated to have been leaked.

Figure 5 shows the discharge rate alongside passing time. In approximately 36.8 minutes, 8 tons of hydrogen fluoride gas are discharged. This calculation method was tested against the GF3 hydrogen tank weight, and showed that 168.8 gal/min and the measured value was 176.6 gal/min. The discrepancy was only 1.7%, making this a valid method.

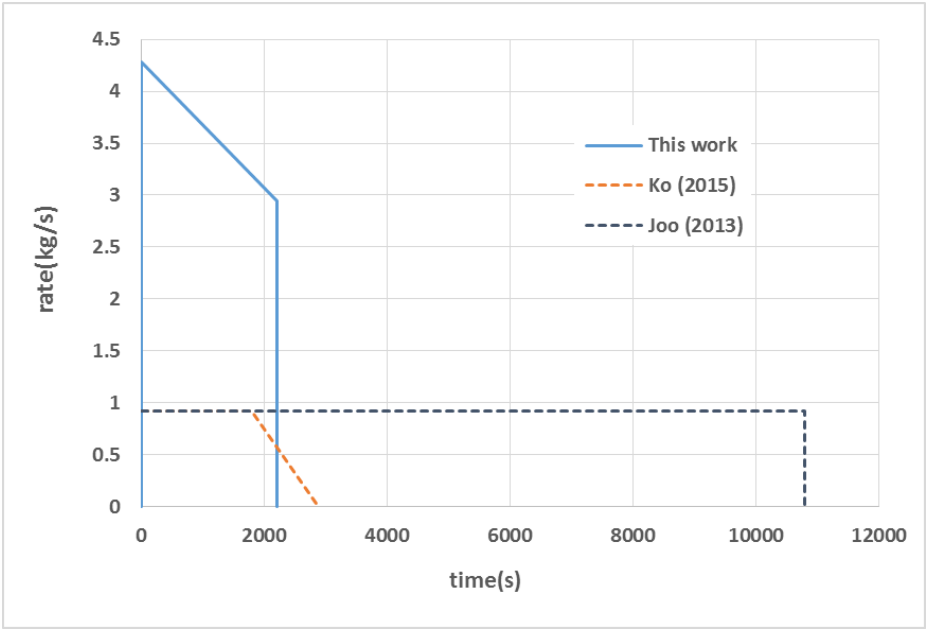

Figure 5 Discharge rate (kg/s) by time (seconds).

2.3.4. Hydrogen fluoride gas leak simulation result

The leak results are shown in Figure 6. Before the leak starts, there is some wind build-up time, which makes a stable wind direction. During the wind build-up time, because of the geometric characteristics of the accident site, the westerly wind slightly changes into a north-westerly wind, moving the clouds towards the south. For the CPU time, it took 299,819 seconds-CPU core. The parallel 12 cores took approximately 6.9 hours to finish the calculation. The leak spread from the industrial complex and moved to the agricultural field.

(a) t = 100 s

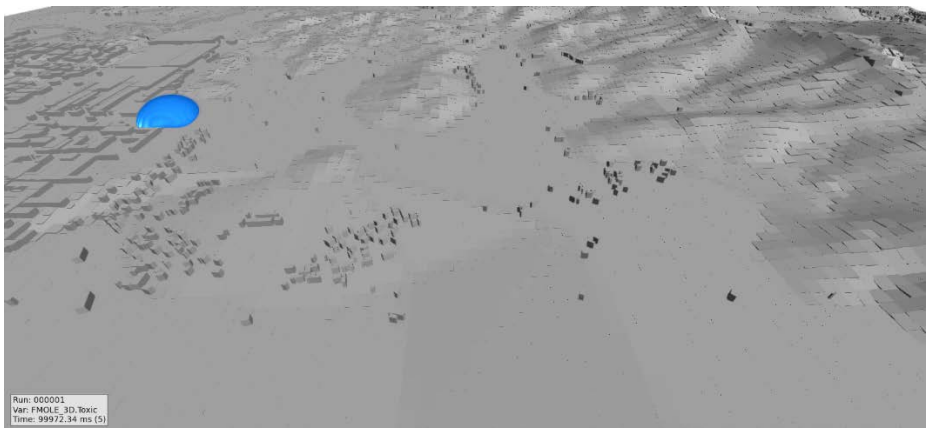

(b) t = 400 s

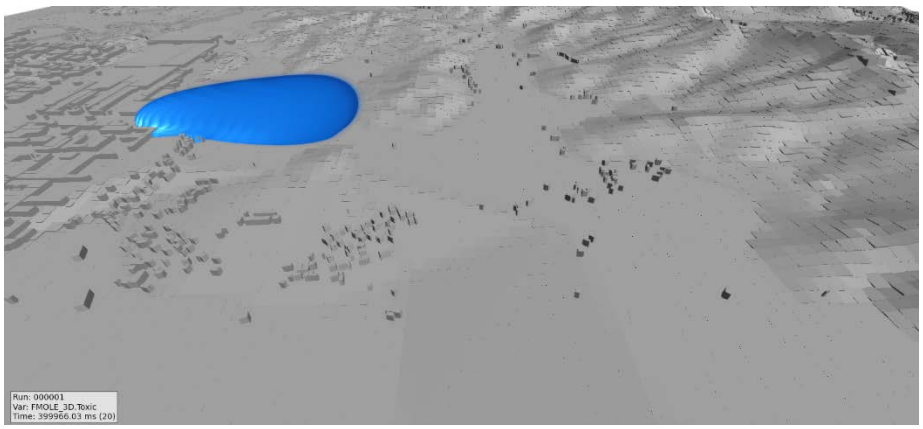

(c) t = 800 s

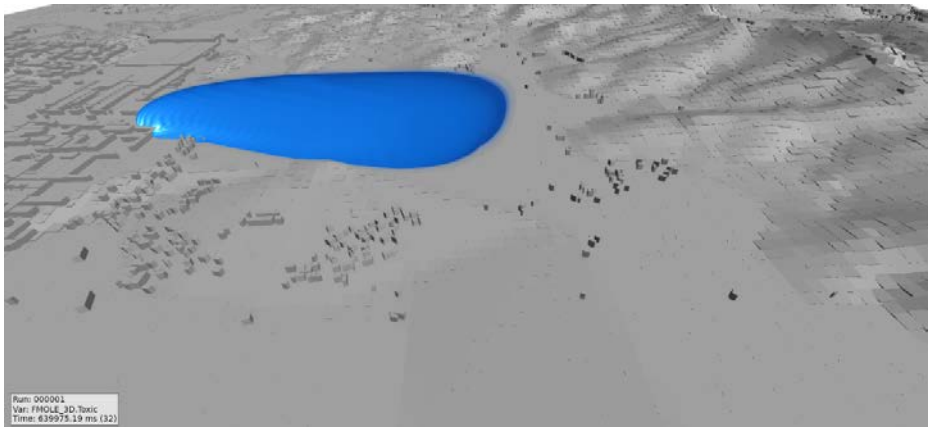

(d) t = 3000 s

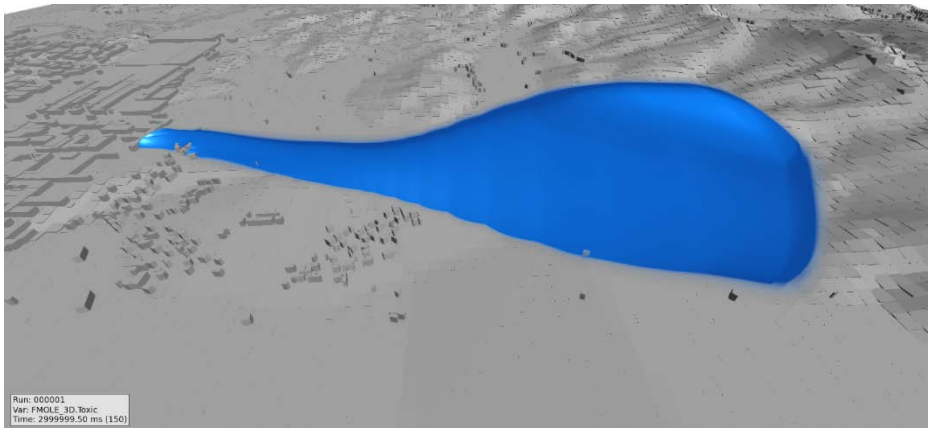

Figure 6 Dispersion (1 ppm) (a) 100 s (b) 400 s (c) 800 s (d) 3000 s

2.3.5. Comparison between the simulation and reported damage

2.3.5.1. Human fatality calculation

Probit was used to calculate the human fatality rate from hydrogen fluoride dispersion.

Probit:

$$\text{Probit} = \text{a} + \text{b}\ \ln \int C^n dt \quad \ldots \text{(Eqn 2-4)}$$

$$P_{death} = 0.5 + (1 + \frac{\text{erf(Probit} - 5)}{\sqrt{2}}). \ldots \text{(Eqn 2-5)}$$

Where, $\text{a} = -8.4$

$\text{b} = 1$

$\text{n} = 1.5$ Probit coefficient (Gexcon AS 2015)

erf: Error function $\text{erf}(x) = \frac{1}{\sqrt{\pi}} \int_{-x}^{x} e^{-t^2}\, dt.$

There were eight people inside the hydrogen fluoride plant at the time of the leak, of which five people died. No deaths were reported outside of the plant. Figure 7 shows the calculated probability of death from exposure to the hydrogen fluoride cloud. The fatality rate is very high inside (~1) the plant with lower values outside the plant, which is an accurate reflection of real events.

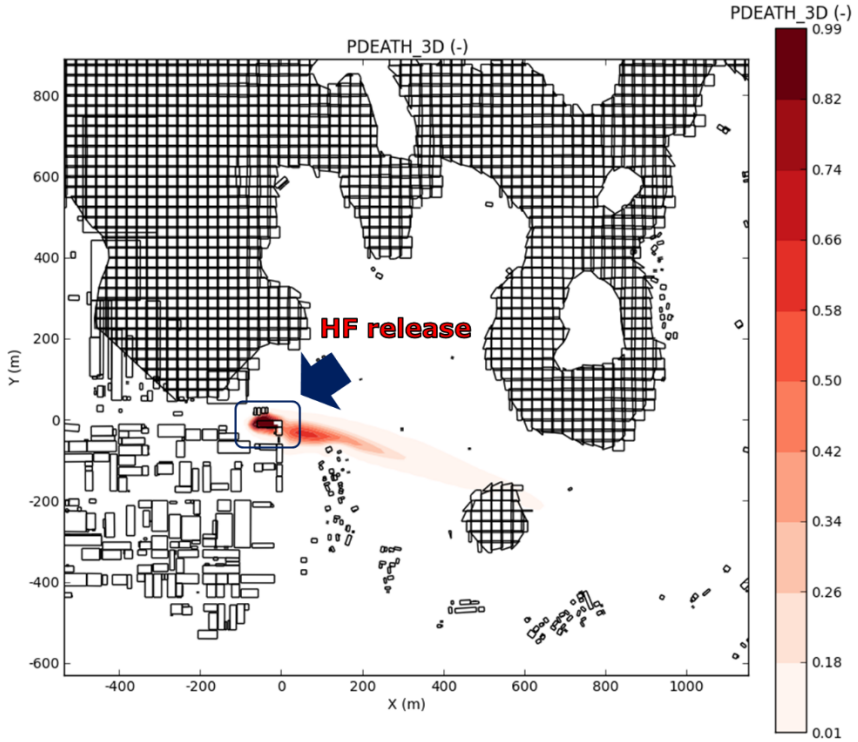

Figure 7 Probability of death by toxic exposure map

2.3.5.2. Applicability of the plant necrosis for post-accident bio-monitoring

For estimating the environmental damage, post-accident data is available in various forms. Some researchers tried to estimate the affected area by using fluoride contents in dead vegetation (Gu et al. 2013; Koh 2014; Yim 2016), fluoride contents in soil (Koh 2014; Kwon et al. 2015), CCTV footage from the time of the accident (Lee et al. 2013), and an optical sensor (Hyun et al. 2013). Among many estimation methods, fluoride content in the vegetation was adopted in this study. Weinstein and Davison (2003) show that the area affected by the hydrogen fluoride leak can be clearly indicated by measuring fluoride concentrations in leaves (Weinstein and Davison 2003).

Gu et al. (2013), Koh (2014), and Yim et al. (2016) gathered vegetation, which had died from exposure to the fluoride around the accident area, and tried to estimate atmospheric concentration levels (Gu et al. 2013; Koh 2014; Yim 2016). All three papers tried to estimate the relation between ambient fluoride concentrations and vegetation fluoride accumulation by empirical dose-rate expression, as seen below.

$$\mathrm{C_{plant}}/\mathrm{K} = \mathrm{C_{air}}\mathrm{T} \quad \ldots \text{(Eqn 2-6)}$$

Where, C_{plant}: accumulation in the plant (mg/kg dry weight);

K: proportional constant

C_{air}: Atmospheric fluoride concentration ($\mu g/m^3$)

T: exposure time (days).

This relation was from long-term, low concentrations (few ppb), making it a good match with some cases, such as an aluminum smelter in Norway (Horntvedt 1997). However, fluoride accumulation by acute fumigation tests is reported not to follow the general patterns observed in chronic exposure and those high concentrations with short duration tests are not enough to make quantitative estimations, unlike chronic exposure. (MacLean et al. 1968; Dogeroglu et al. 2003) Furthermore, the proportional constant K in the equation has a wide variability, with reports varying from 0.4 to 7.7 for the same species. There are several reasons for this variability, such as dependency on climate, position in the trees, and some individual differences (L.H.Weinstein and A.W.Davison 2004). Thus, estimating airborne fluoride levels by this relation should be used with care. Table 2 and 3 shows the source data point.

Table 2 Environmental damage data reference

Distance from the source	Direction	Collection date	Maximum estimation	Reference
Within 1km	Most damaged (ESE)	After 10 days	14.69 ppm	Gu et al. (2013)
Within 3km	All direction	After 2 weeks	3.06 ppm	Koh et al. (2015)
Within 5-20m	Near source	Within 1 day	3.55 ppm	Yim et al. (2016)

Table 3 Detail data of HF accumulation

No.	Distance	Species	Conc.	K	Conc.	No.	Distance	Species	Conc.	K	Conc.
1-1	212	Rice	9594	0.78	12300	1-13	603	Fir	626	0.31	2020
1-2	254	Rice	1311	0.78	1681	1-14	644	Rice	783	0.78	1004
1-3	315	Melon*	998	2.5	399	1-15	710	Plum	304	0.99	307
1-4	316	Persim-mon	3407	1.07	3184	1-16	928	Jujube	134	1.07	127
1-5	320	Melon*	835	2.5	334	1-17	943	Rice	140	0.78	180
1-6	328	Melon*	1575	2.5	630	1-18	989	Rice	142	0.78	183
1-7	361	Pine	292	0.24[1)]	1217	2-1	278	Pitch Pine	462	0.3	1540
1-8	366	Soy bean	5224	2.23	2343	2-2	587	Nut Pine	584	0.3	1948
1-9	393	Grape	1002	2.5	401	2-3	676	Pine	477	0.3	1590
1-10	407	Chilli pepper	1873	1.14	1643	2-4	1046	Pitch Pine	32	0.3	108
1-11	456	Perilla	2823	2.23	1266	2-5	1530	Pine	21	0.3	71
1-12	508	Radish	1253	2.23	562						

Gu et al. (2013) collected dead plant matter from the most damaged area. Through personal communications with the author, it was learned that 16 out of 24 were used by ruling out the vegetation in the greenhouse and missing vegetation positions. Koh et al. (2015) collected only the plants among the pines, and revealed the longitudes and latitudes of the collection points.

2.3.5.3. Kriging method

The Kriging method was used to estimate the approximate damaged area. For the estimation purpose, the MATLAB Kriging toolbox Design and Analysis of Computer Experiment (DACE) was used (Lophaven et al. 2002). Kriging is a method of interpolation through Gaussian process regression.

All three references in Table 2 used an exposure time of 1 day without a concrete reasoning process. This 1-day averaging assumption is very conservative, meaning it would function as the minimum value. It is very hard to determine actual vegetation exposure time; therefore, the toxic dose was used instead of atmospheric concentration. The toxic dose is defined as the product of concentrations in air and time. More than 3 km from the emission source shows low accumulation in the leaves; therefore, it is assumed that there exists a low dose (<0.01 mg/m^3*min) in all directions.

2.3.5.4. Environmental damage

Figure 8 shows the toxic dose contour simulated by CFD around the leak site. Black dots represent the dead vegetation collection positions. A hydrogen fluoride cloud footprint follows the environmental damage. This contour is based on the z = 1.5 m to represent approximate human size so that some points with buildings or hills that are higher than 1.5 m are not shown in the figure, resulting in interference with some contour lines. When comparing actual and simulated dosages, simulated dose is 6-7 times greater.

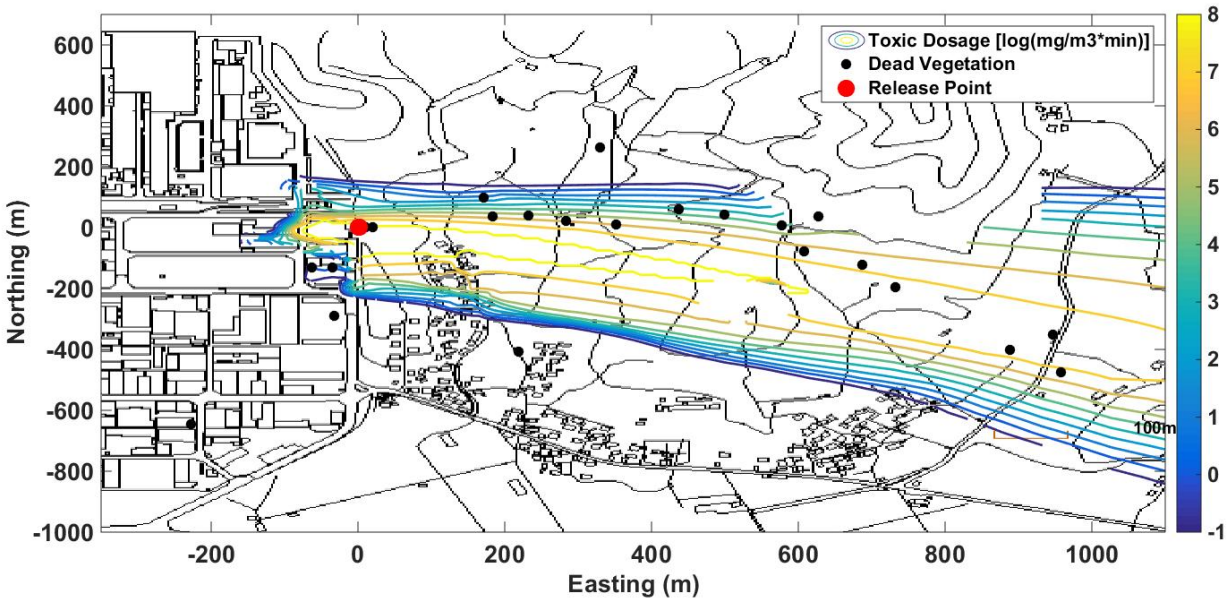

Figure 8 Toxic dose contour

As stated above, vegetation damage was simulated by toxic dose. In Figure 9 the blue contour, derived by applying the Kriging method, indicates a toxic dose of 100 mg/m^3*min. The magenta contour is derived from the CFD simulation for the same dose. For the downwind direction, east of the release point, the estimated damage area based on vegetation has a boundary similar to that based on simulation, while the upwind direction does not show an exact match. This mismatch is because this study does not consider wind direction change with time. Still, as can be seen in Figure 3, a northwesterly wind and southeasterly wind were the second common wind directions so that downwind concentration would be overestimated and upwind direction would be underestimated.

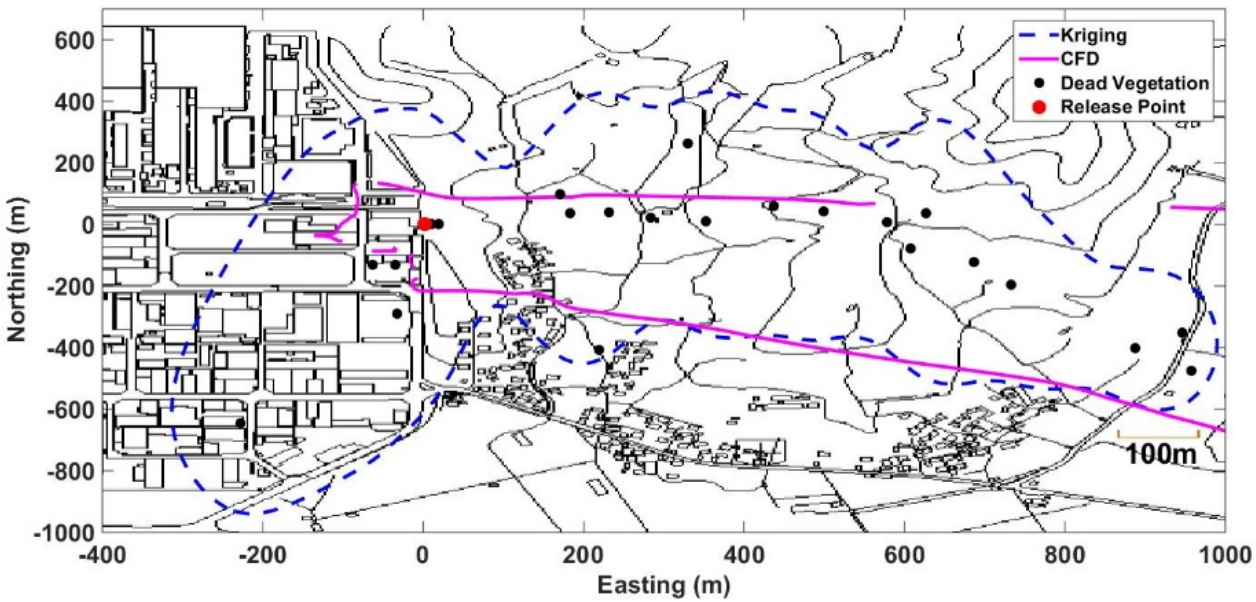

Figure 9 Map of 100 mg/m3*min dose equivalent for Kriging and CFD result

2.4. Chapter conclusion

The purpose of this study was to construct a CFD model that can interpret toxic gas dispersion, based on an actual hydrogen fluoride leak that occurred in 2012. To construct a valid model, anhydrous hydrogen fluoride dispersion was tested, with results showing a mean relative bias of 0.336 and mean relative square error of 0.134, which is within an acceptable range according to LNG dispersion protocol. With the anhydrous ammonia test, some dispersion models were compared and this CFD model showed quite a good match with the test.

Hydrogen fluoride accidents were reproduced using this computational fluid dynamics model. The results reproduced the actual human fatality at a high range as well as downwind vegetation damage. Therefore, it was concluded that the CFD for toxic cloud dispersion has some advantages, such as concrete geometry modeling.

Chapter 3: Chlorine dispersion CFD model in an urban area

3.1. Chapter outline

Computational Fluid Dynamics (CFD) is widely used to simulate accidental toxic chemical releases due to easier application for various conditions with geographic obstacles presence which other simpler models cannot handle. Some of the previous simulations are done near release sources like industrial sites (Zhang et al. 2013, Dharmavaram et al. 2005), near pipelines (Mazzoldi et al. 2011), and indoor (Siddiqui et al 2012) etc. With the development of the computing technology, chemical release scenarios in the urban area become possible.

Tominage et al. (2013) reviewed CFD simulation of the near-field pollutant dispersion in the urban environment. Hanna et al. (2009) simulated hypothetical chlorine release in the Chicago, then Sanchez et al. (2013) used the CFD simulation to couple with exposure model. Zheng-Tong et al. (2009) used Large-eddy simulation (LES) to model the case in London. M. Lateb et al. (2011) showed pollutant dispersion in the wake of a building in Montreal. Hanna et al. (2006) compared 5 commercial CFD codes to simulate New York City wind pattern with flow obstacles.

Motivated by these literature, this chapter deals with CFD simulation of chlorine accidental release in urban area with different weather conditions to find the worst case, then simulation is accelerated with increasing Courant-

Friedrich-Levy number and parallel solvers. For the selected worst case, one-hour simulation and probability of death of the vulnerable points are shown.

3.2. Background

3.2.1. CFL number

The numerical time step calculation algorithm which is used in FLACS is based on implicit first-order backward Euler method. Time steps in transient simulations should be set so that the solution evolves smoothly and stably in time. The Courant-Friedrich-Levy (CFL) number is used to give a solver-specific criterion for the maximum time step that gives a stable solution in the compressible solver of FLACS. Two CFL number are used to determine the maximum time steps. CFLV is a CFL number based on fluid velocity while CFLC is a CFL number based on sound velocity. CFD solver chooses minimum value between CFLV and CFLC.

$$\Delta t_V = \frac{CFLV}{max\left(\frac{u_i}{\Delta x_i}\right)} \quad \ldots \text{(Eq. 3-1)}$$

$$\Delta t_C = \frac{CFLC}{max\left(\frac{c}{\Delta x_i}\right)} \quad \ldots \quad \text{(Eq. 3-2)}$$

$$\Delta t = min(\Delta t_V, \Delta t_C) \quad \ldots \text{(Eq. 3-3)}$$

To the best knowledge of the authors, there isn't any toxic gas dispersion related CFD simulation with CFL evolution technology. CFL evolution techniques such as exponential progression, switched evolution relaxation, residual difference method can be found in Bücker et al (2009). For exponential progression, typical exponent value lies between 1.05 and 1.5. Efficient convergence can be achieved by large global CFL number while robustness is maintained by limiting local CFL number. (Chenzhou Lian et al. 2009) Still references claim that these methodologies are solution-limited and generally not determined *a priori*.

3.2.2. Chlorine toxicity calculation

Chlorine is handled on a large scale in liquefied form for the industrial purposes. It is one of the major toxic hazard materials. Although there are many possible ways to calculate chlorine toxic consequence, this research uses method from Withers and Lees (1985). The vulnerability model describes average fatal effects for population model due to chlorine. Trapezoidal numerical integration method was used to integrate numerically.

$$\Pr = -8.29 + 0.92\, ln \int C^2 dt \quad \ldots \text{(Eq. 3-4)}$$

$$P_{death} = 0.5 + (1 + \frac{\mathrm{erf}(\Pr - 5)}{\sqrt{2}}) \quad \ldots \text{(Eq. 3-5)}$$

$$\int_a^b f(x)dx \approx \frac{1}{2}\sum_{k=1}^{N-1}(x_{k+1} - x_k)(f(x_{k+1}) + f(x_k)) \quad \ldots \text{(Eq. 3-6)}$$

Where, Pr: Probit

C: Concentration in ppm

t: time in minute

erf: error function

P_{death}: Probability of death

N: Number of time steps

3.3. Method

3.3.1. Data acquisition

One of the industry complexes in the Republic of Korea was chosen for an accidental chlorine release. The Mipo complex in Ulsan metropolitan city has about nine hundred factories and one hundred thousand workers[16] and is adjacent to the large residential area, thus might cause severe consequences when it comes to toxic chemical release. Two dimensional geometry CAD file was acquired from National Spatial Information Clearinghouse (NSIC). Figure 11 shows satellite image of the area from Google Earth and Figure 12 is 2-D CAD image of the area. Southeast part of the area is for industries and northwest part is for residences. The hypothetical release source is a hydrogen-chloride production factory, which uses hydrogen and chlorine as reagents. Longitude and latitude of the source is around N35.5, E129.3, and actual coordinate is hidden due to protection of the company. And building height data was from Vworld database, and mountain height was simplified as cylinder of 10m since concentration on mountain is none of the research concern. There

are 3 elementary schools and 2 nurture schools within the simulation volume, and they are considered as vulnerable points in this study.

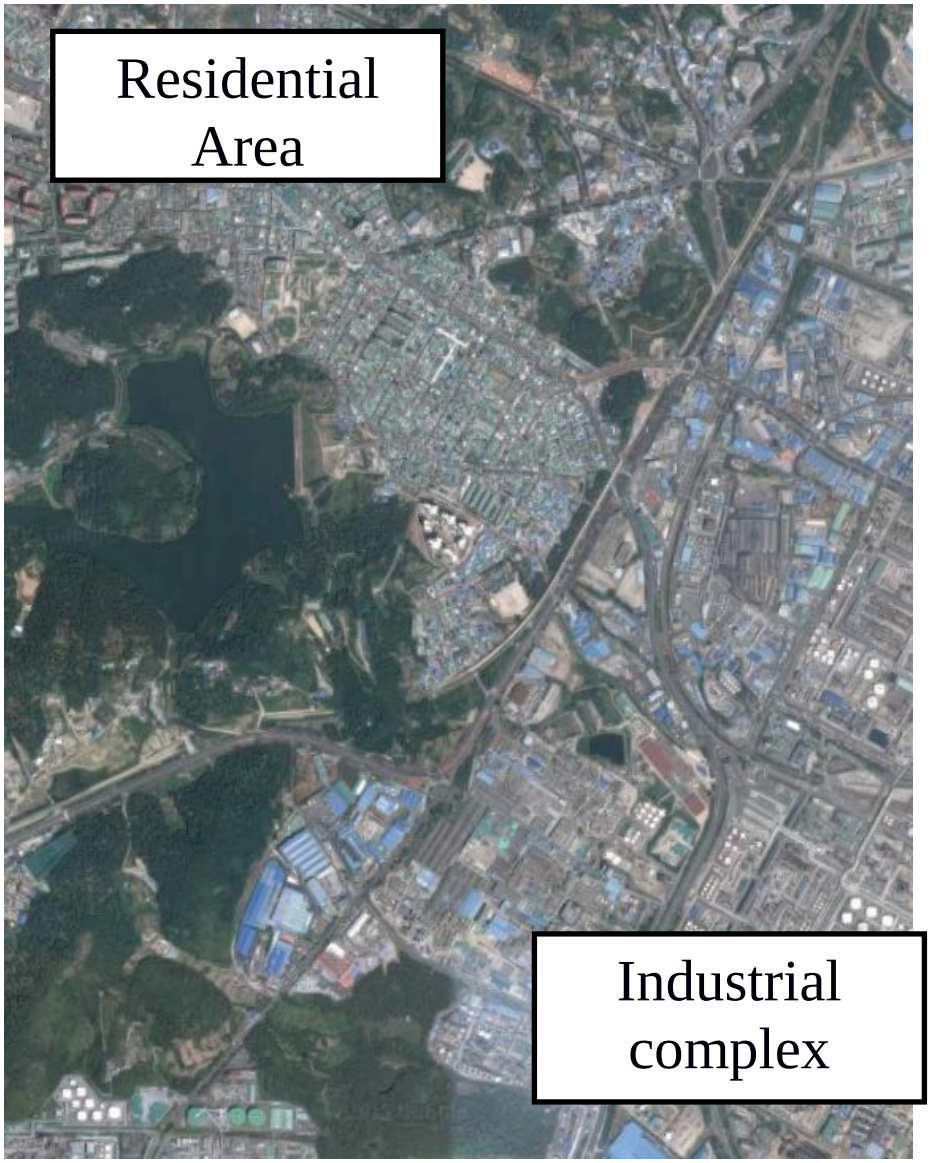

Figure 10 Satellite image of the area

[Google Earth Image]

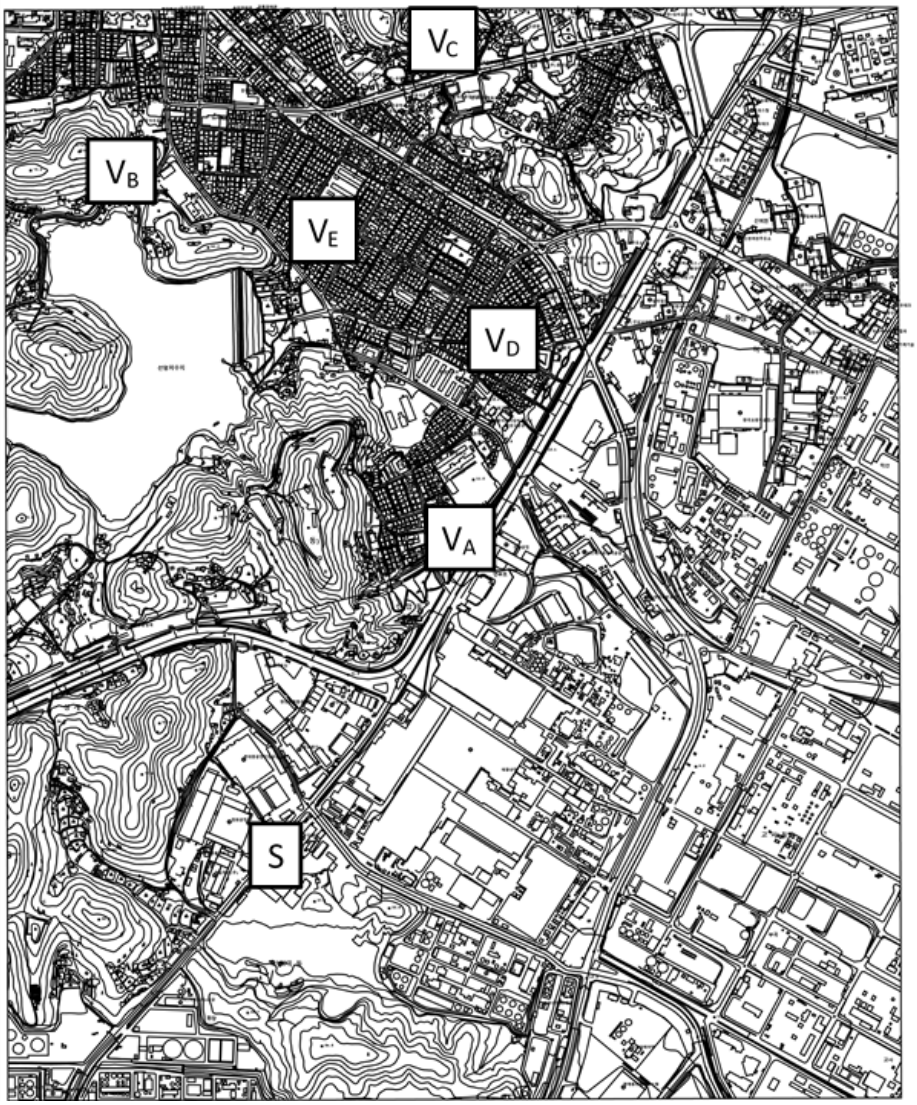

Figure 11 CAD file image of Area

S stands for source and VX stands for vulnerable points

3.3.2. CFD simulation setting

3.3.2.1. Input parameter setting

A hydrogen chloride plant is chosen for the source of the chlorine release. The manufacture company passed gas safety test successfully thus this case is purely hypothetical. It is located in (x, y) = (50, -1730) in the geometry. For the geometry, x-direction is east (+) to west (-) and y-direction is north (+) to south (-), z-direction is height from ground level. The way how to make grids is a key to successful CFD simulation. Information of the grid core and stretched is shown in the table 4. Minimum cell size is 6m by 6m by 2m according to Hanna et al (2009) chlorine release simulation. For initial 10-minuets dispersion scenario, 10 cases were selected with normal wind speed (3m/s) and the worst case wind speed (1.5m/s) and 5 wind directions which is clockwise 45 degrees from east wind to west wind. Chlorine leak is 50kg/s and 60s duration.

Table 4 Core and stretched domain gridding

Core Domain	*x*	*y*	*z*
Minimum	-151m	-1931m	0m
Maximum	251m	-1529m	20m
Cell size	6m	6m	2m
Number of Cells	67	67	10
Stretched Domain	x	y	z
Minimum	-500m	-2500m	0m
Maximum	1000m	500m	80m
Max Factor	1.2	1.2	1.2

3.3.2.2. Calculation setting

Each of the simulation is done by parallel computing of five CPU threads. The computer used in this research has 2.7GHz/24 Core CPU cores and 256 GB DDR3 RAM. After finding fast and robust time step, how the number of cores affects simulation speed was studied up to 20 cores.

3.3.3. Time step increase method

Firstly, initial CFL number sensitivity analysis was conducted to find the fastest result while keeping robustness of the simulation. CFLC number is chosen over CFLV number because CFLC number was the primary time step limit. CFLV number is set to 1/10 of the CFLC number. The value that is suggested by FLACS software is 5 and we increased the value uniformly to reach the number with which the mass residual is too large to simulate continuously. Large time step size weakens numerical stability.

Secondly, CFL increase with time was tested. Since the exponential increasing of CFL number damaged the simulation robustness severely even when small exponential ratio was used, linear increasing after the release completion was applied. The linear increasing scheme is like below. The CFL slope k, or final CFL number was test for sensitivity to find appropriate stiffness.

$$CFL = CFL_0 (when, t \leq t_0) \quad \ldots \text{(Eq. 3-7)}$$

$$CFL = CFL_0 + k(t - t_0)(when, t > t_0) \quad \ldots \text{(Eq. 3-8)}$$

Time of CFL number change (t_0) is set to 100s as the release stops at t = 60s.

3.3.4. Classification method

Based on the 12 case that varies release rate, wind speed and direction, neural network classification model was trained. For the first 10 minutes from the release start, 1 minute sampling time was applied. Only the z=1.5m result was used to reduce the size of the training. Then, total data point is 3,633,120. And all of the points by time was classified into 4 classes and then 2 classes. Sample dataset is visualized as figure 13. Training set is 70%, validation set is 15%, and testing set is 15%.

Class 1 is concentration below ERPG-1. Class 2 is concentration between ERPG-1 and ERPG-2. Class 3 is concentration between ERPG-2 and ERPG-3. Class 4 is concentration above ERPG-3. When classified into 2 classes, class safe is concentration below ERPG-2, which is common endpoint in toxic gas simulation. Class danger is concentration above ERPG-2.

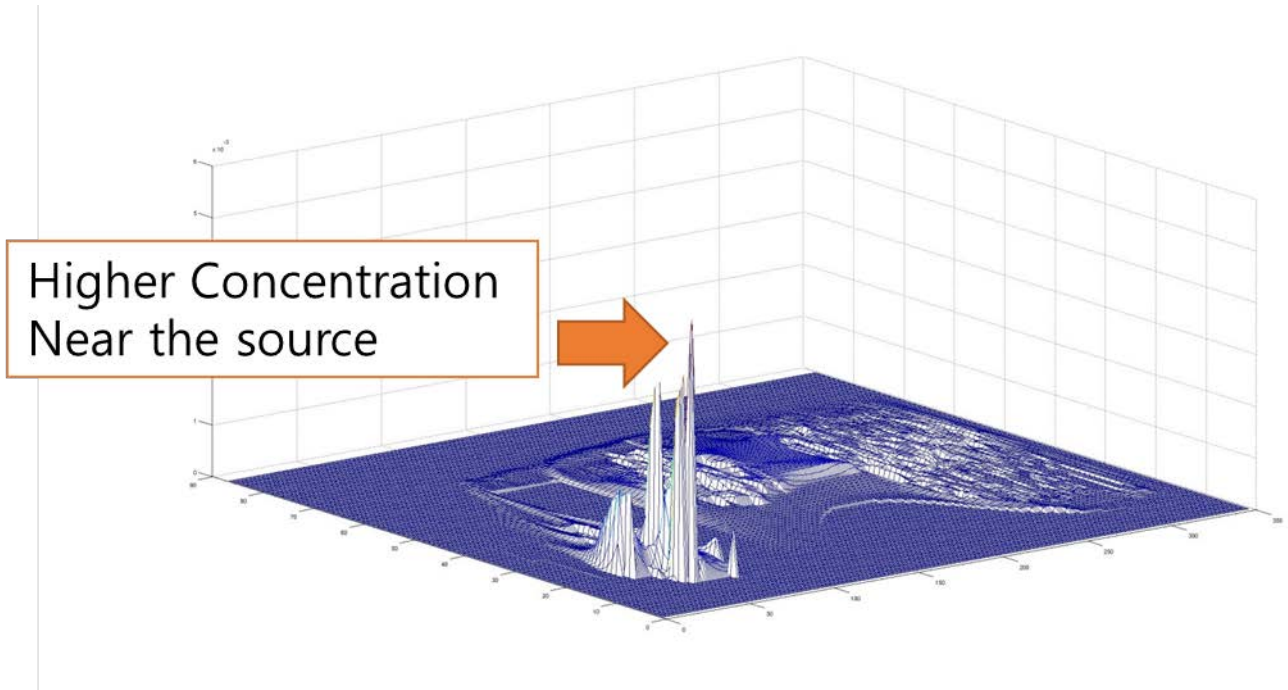

Figure 12 Sample dispersion concentration data

3.4. Result and discussion

3.4.1. Case study result

Figure 14 shows 10 case studies of the first 10 minutes. Wind direction is (a) East, (b) Southeast, (c) South, (d) Southwest, and (e) West from left to right. And upper cases are for the (1) normal wind speed (3m/s) and (2) lower cases are the worst wind speed (1.5m/s). Blue color means ERPG-2 (20ppm) and red color means ERPG-1 (1ppm). The case (c2) was the chosen as the worst case as the chlorine is heading toward residential area and lower wind speed typically indicates higher danger level. For the worst case scenario, total 1 hour was simulated and vulnerable points' consequence was calculated. Table 5 shows the probit and probability of death. It shows 3 out of 5 points are extremely dangerous when the worst chemical release occurs.

Table 5 Probit Calculation Result

	A	*B*	*C*	*D*	*E*
Probit	9.4486	-2.7406	6.07157	7.1376	0.3638
Probability of Death	99.9996%	0.0000%	95.6898%	98.3726%	0.0002%

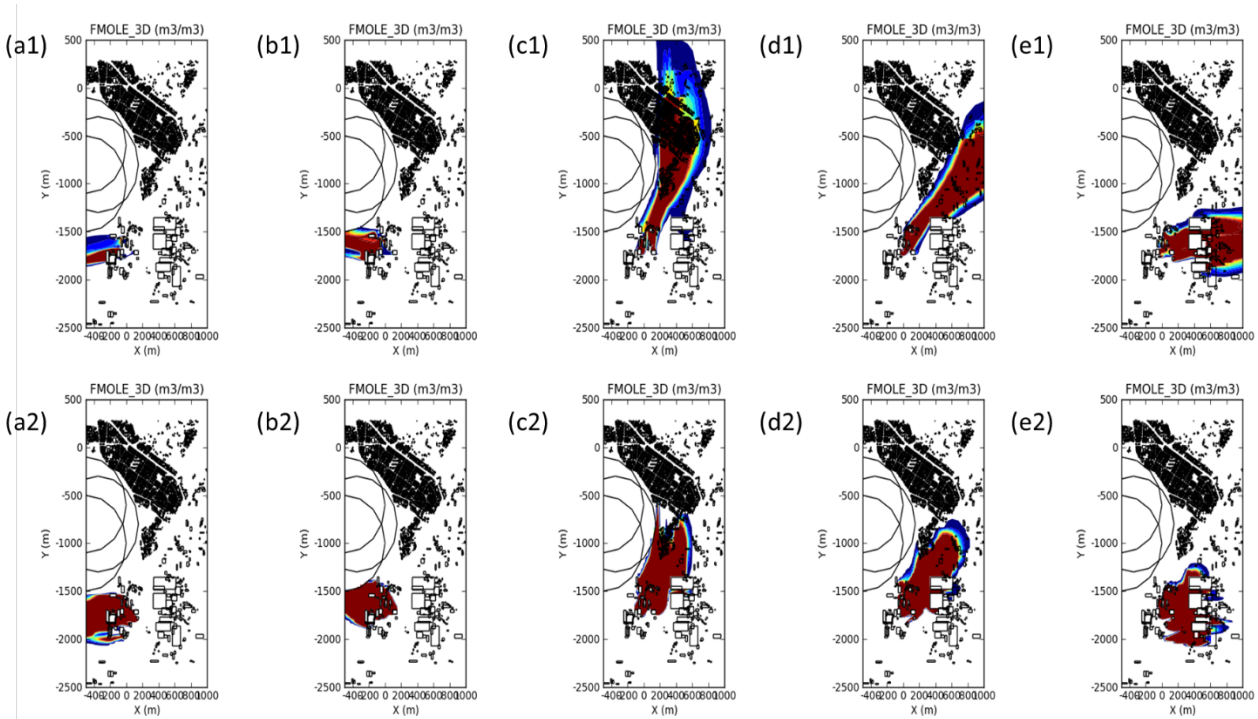

Figure 13 Case studies for weather condition

3.4.2. Time step change result

Figure 15 shows the results of the sensitivity analysis. The CPU time and number of time step is decreasing along with increasing CFL number. When CFL number gets over 10, the simulation aborted due to large mass residual. Figure 16 shows time step decreasing with final CFL number on the x-axis. Initial CFL number is 10 as it is the maximum limit that allows stable simulation

Figure 17 shows how much time is taken to simulate the case over the number of parallel solvers. It shows that parallel solving with more than 13 solvers didn’t result in faster solution. Table 6 shows final results. Time consumption decreased by almost 4-fold

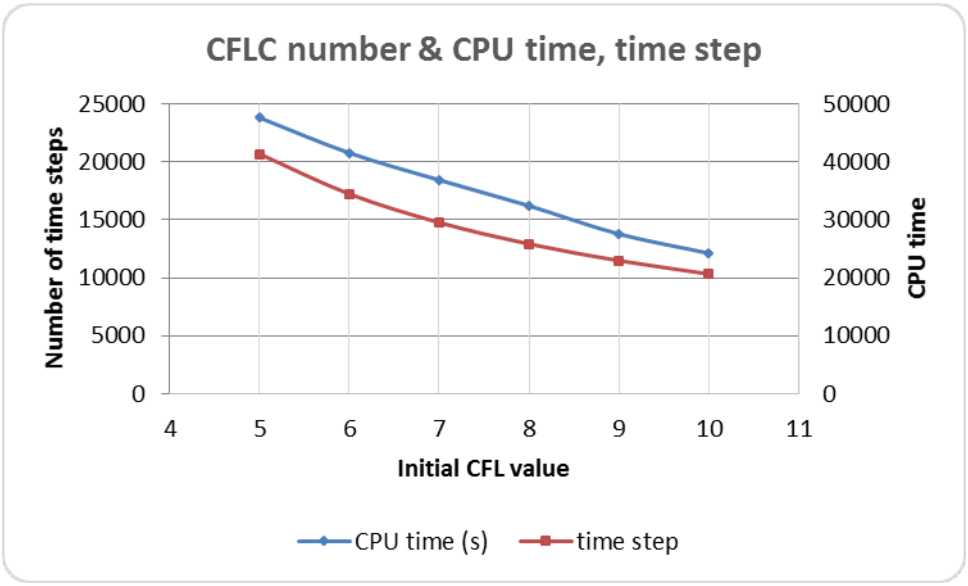

Figure 14 CPU time and number of time steps by CFL number.

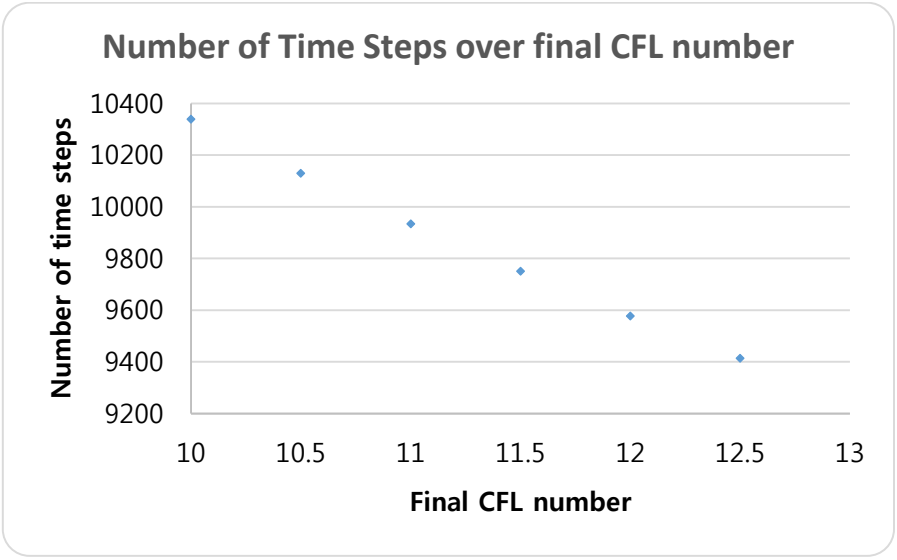

Figure 15 Number of Time Steps over Final CFL number

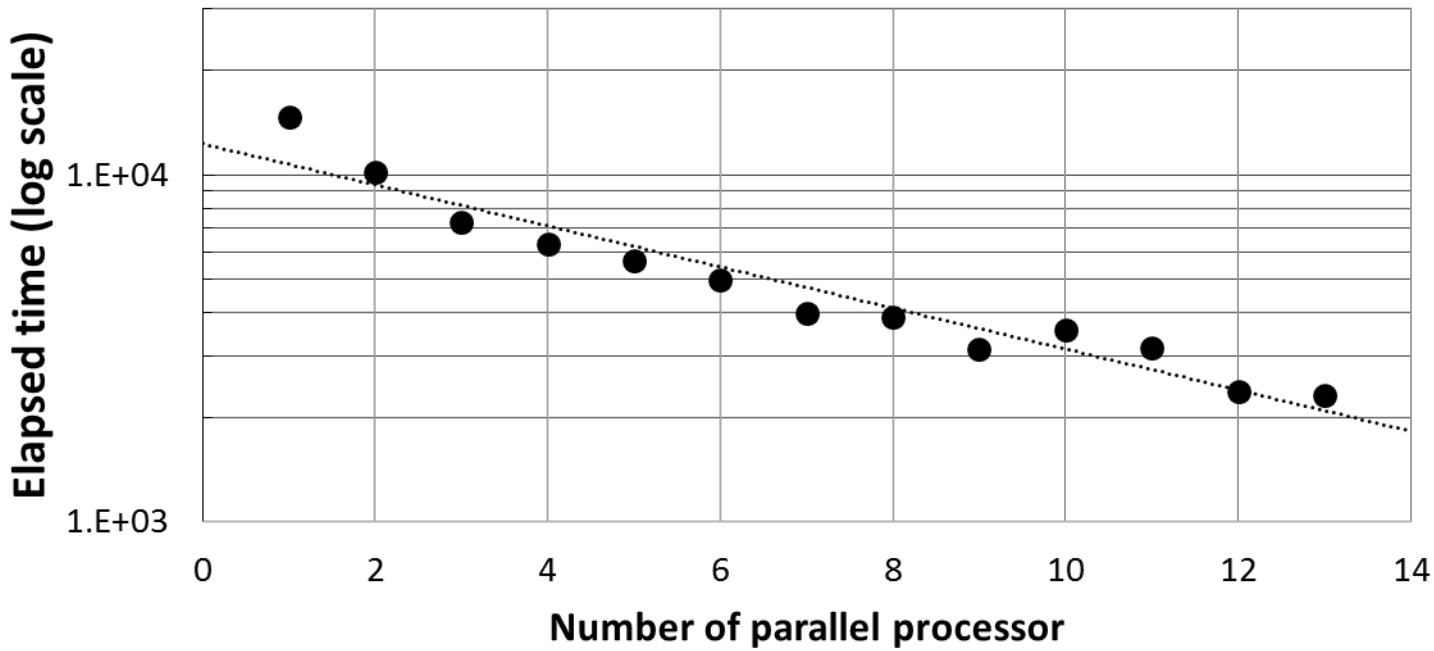

Figure 16 Elapsed time over number of parallel solver

Table 6 Result of the CFL search and parallel solvers

	Initial CFL	Final CFL	Parallel Solvers	time steps	CPU time	Elapsed Time	Relative Time
FLACS suggestion	5	5	5	20677	47602	9520.5	100.0%
CFL sensitivity	10	10	5	10339	24248	4849.5	50.9%
Linear Increasing Method	10	12.5	5	9414	18490	3698.0	38.8%
Parallel solver	10	12.5	13	9414	30199	2323.0	24.4%

3.4.3. Classification result

Figure 18 is Relative Operating Curve (ROC) of the ANN. All of the sets including a training set, a validation set, and a test set shows true positive rate is higher and well classified. Class 1 and 4 is relatively well-classified than middle ranged classes 2 and 3. Table 7 shows confusion matrix. Overall accuracy is 92.3% and that could mean neural network classification can reproduce the CFD result, however, this is typical type of unbalanced problem which class one has the most data. Neural network training tends to fit the data to make total accuracy higher. When classified into 2 classes, class safe and class danger, total accuracy goes to 95.6% and did not show the tendency to fit data to safe side.

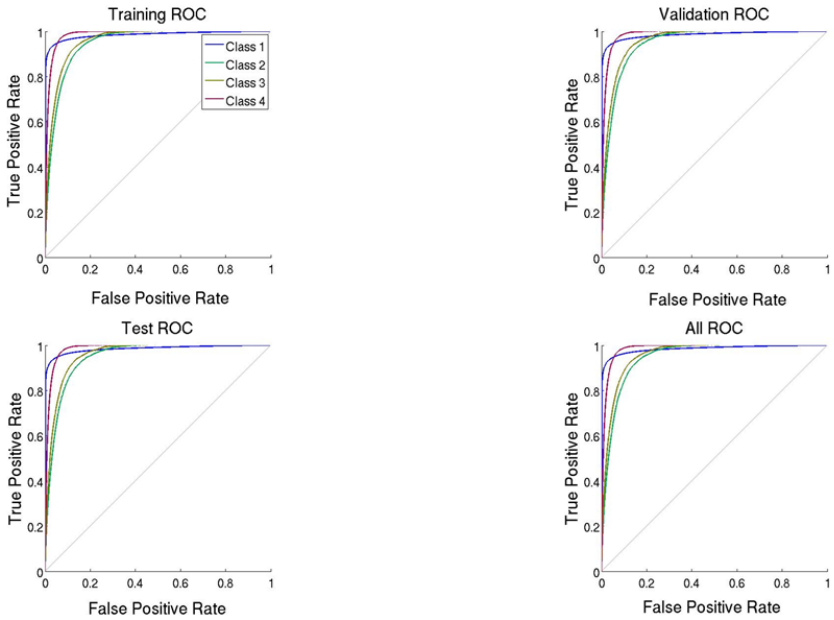

Figure 17 Relative operating curve of neural network classification

Table 7 Classification result of 4 classes

	Target	**1**	**2**	**3**	**4**
Output	Accuracy	97.5%	3.1%	36.5%	88.7%
1	96.1%	2,908,834	38,859	43,677	35,504
2	47.7%	1,082	1,969	1,061	19
3	54.8%	14,359	15,705	53,567	14,163
4	77.3%	59,029	6,847	4,8515	389,930

Table 8 Classification result of 2 classes

	TARGET CLASS	**SAFE**	**DANGER**
OUTPUT CLASS	Accuracy	97.0%	88.1%
SAFE	97.7%	2,955,558	69,562
DANGER	85.0%	91,126	516,874

3.5. Chapter conclusion

As the Republic of Korea has large population density so that residential area is affected by the release of toxic chemical in the industrial area easily, computational fluid dynamics can help figure out how severe the consequence would be, thus how much protection and regulation is needed. To overcome the drawback of the CFD, calculation time can be reduced using numerical time stepping method and parallel solvers.

First, the vulnerability model used in this chapter might have underestimated the risk. The probit model takes general population as Gaussian distributed, and children and elderly are more vulnerable. So the probability of death is smaller value than reality.

Second, the CFL evolution technology is still solution limited. Although 10 case studies were able to run even though the evolution initially tested in one scenario, it is not known that it can be applied generally. When stronger winds were tested, the simulation went quite unstable. Grid refinement around the leak can help make simulation stable even when large CFL number is used, though it creates smaller grid to lead to smaller time step.

Lastly, in this study parallel solvers did show certain limit, however it is widely known that it helps simulation faster. That is partially because y-directional sub-block division made calculation load more, but more threading will eventually get simulation faster. This study left that as a future work when more computing ability is ready.

Chapter 4: Detector allocation optimization using CFD

4.1. Background

4.1.1. Detector allocation problem

Some previous works contributed to gas detector allocation using CFD. There is certain general principles of gas detection, such that set point of point detectors should be set between 10% and 25% on low alarm and 30% and 60% on high alarm, based on lower flammability limit (LFL). (Davis et al. 2011) And Richart et al. used eight CFD scenario simulation along with wind direction, 45° aside each, and assuming the worst case scenario to determine gas detector allocation. (Richart et al. 2006)

Also, there are some researches regarding gas detector position optimization, based on the work of Berry et al. (2006), which founded the basic structure for sensor placement optimization with municipal water networks. S.W. Legg et al used a stochastic programming approach to optimize gas detector dispersion simulations using CFD. (Legg et al. 2012) They proposed the Mixed Integer Linear Programming (MILP) problem formulation (SP), problem with coverage constraint (SPC), only with coverage constraint (C), and later they considered conditional-value-at-risk (CVaR) when placing gas detectors. (Legg et al. 2013) A.J. Benavides-Serrano et al. extended work of S.W. Legg et al. with unavailability (SP-U) and voting strategies. (SP-UV)

(Serrano et al 2013) The optimization method is further developed considering Quantitative Assessment (Serrano et al. 2015), and P-median formulation (SPqt) (Serrano et al. 2016). References calculated 270 release scenarios with a CFD software, FLACS and 994 potential point detector locations in the real, medium-scale (50m x 70m x 20m) geometry. Gomes et al. (2004) used 32 scenarios (2 location, 2 release direction, 8 wind direction) to solve similar problem.

The number of different scenarios affects quality of the optimization solution a lot. When using a small number of scenario relative to the number of potential detector position, allocated detectors tends to gather together near the each source in the scenario setting and does not guarantee fine optimization. Still, a large number of scenario simulation in CFD takes too much computational resources.

4.1.2. Surrogate model with CFD

Surrogate model technology make it possible to conduct a computer-aided experiment such as CFD. There are many former researches to formulate a surrogate model for CFD in application for aerospace simulation and mechanical engineering. For the field of chemical safety application, Ke Wang et al. (2014) made basic LNG vapor cloud dispersion model with the help of Hamersley sampling, FLACS CFD engine, segmented principal component transform-principal component analysis (SegPCT-PCA), and Gaussian process

regression (GPR). And Luca et al. (2016) used c-APK technology (anchored-ANOVA-POD/Kriging) for uncertainty analysis of CFD model for toxic gas simulation in the urban area. These two papers showed that surrogate model based on the CFD model for application in chemical safety field is possible. This chapter deals with one of the application area in the chemical safety, which is detector allocation problem.

4.2. Method

The main idea of this chapter is that building meta-model based on some of CFD results can predict other CFD results so that this meta-model can be used to optimize a detector layout in a petrochemical plant. To avoid the high computational burden, the number of the CFD simulation should be reduced.

First step for meta-modelling is called Design of Experiment (DoE). Here Latin Hypercube Sampling (LHS) is used. LHS is a kind of space-filling method and considered as commonly used metamodeling techniques. (Hamel et al. 2006) For meta-model choice and fitting method, the Artificial Neural Network (ANN) regression and back propagation is used.

Overall procedure of this chapter is in Figure 19. First, design of experiment is done using LHS to find M_1 scenarios with 5 different input variables. Then, all scenarios are solved via CFD to find the sensor detection time. The CFD results are gathered and sent to make a meta-model using ANN. This model is cross-validated and used to model M_2 new cases. Total $(M_1 + M_2)$ scenario result is now basis of MILP and then optimum detector location is obtained. In

this research, $N_1 = 30, and\ N_2 = 100$ is used to maintain a reasonable number of CFD simulation and to avoid situation that number of potential detector location is too larger than the number of leak scenarios.

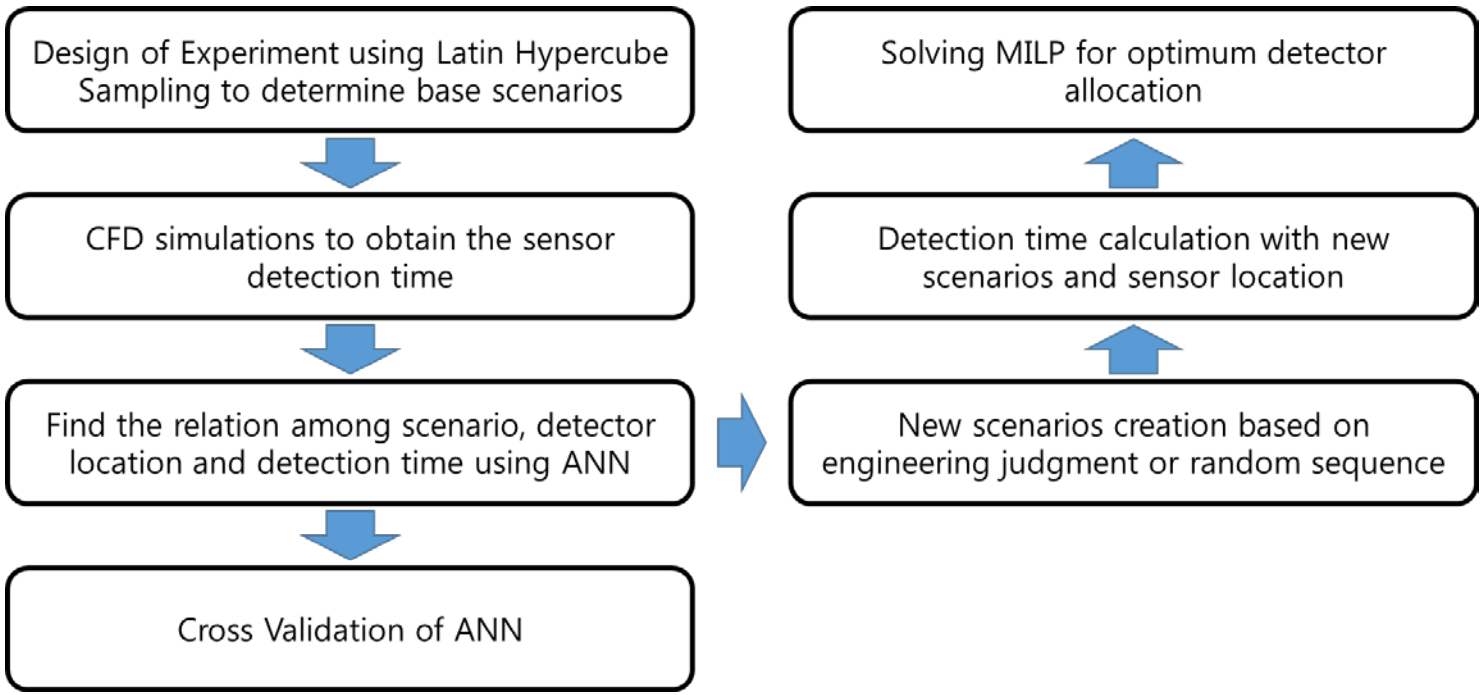

Figure 18 Procedure of detector allocation optimization with metamodelling

4.2.1. CFD Setting

Total five variables were selected as scenario inputs, which can be divided in two categories. Meteorological inputs are U_x and U_y, which are wind velocity along with East (+x) - West (-x) and North (+y) – South (-y) respectively. Minimum and maximum value of the wind velocity in each direction is $\pm 3.5 \mathrm{m/s}$, which can make wind speed up to about 5 m/s. Leak inputs are $\dot{m}, S_x, S_y$, which stands for mass rate(kg/s), location of leak in x (m) and y (m) direction respectively.

Figure 20 shows Latin Hypercube Sampling (LHS) result. Each dot represents the release spot in x and y coordinate, while the size of the spot shows size of the LNG leak. The arrow from each spot means wind direction of the scenario. For scenario number 6 and 27, y coordinate was adjusted by -4 m and +4 m, respectively to avoid geometry interference of leak source. Table 10 shows data sample used.

Figure 21 shows geometry of an LNG terminal, the geometry file (co-file) is from FLACS best practice, pool spread simulation. Composition of LNG is methane 95%, ethane 4%, and propane 1% all in volumetric percentage. In the core region, 1 m x 1 m x 1m grid was used and it grows by the factor of 1.2. Total number of grid in each simulation is 196,236. The potential location of sensor is 1587, which is in array of 23 in x, 23 in y and 3 in z direction.

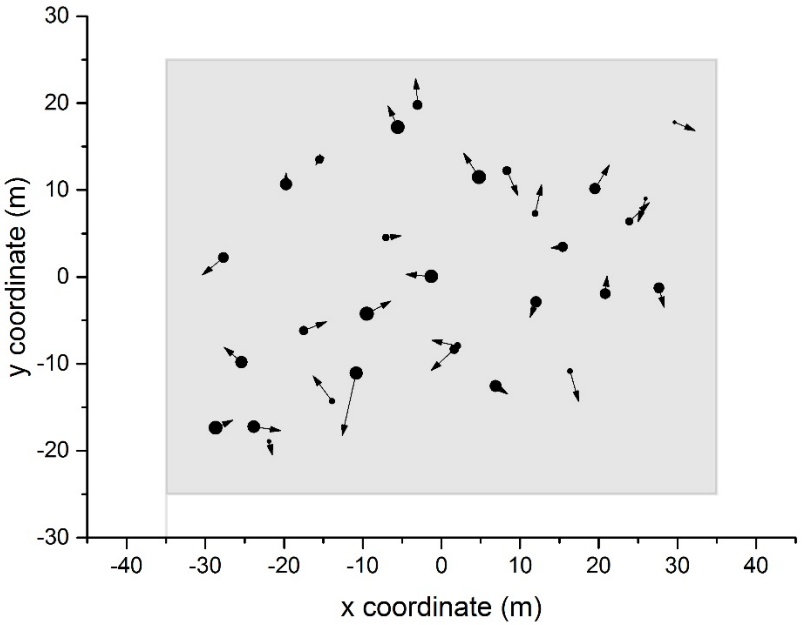

Figure 19 LHS for 5 variables

Position of a dot represents leak source position, size of a dot represents mass flow rate, and length and degree of the arrow from a dot represents wind speed and direction. Light grey area is process are

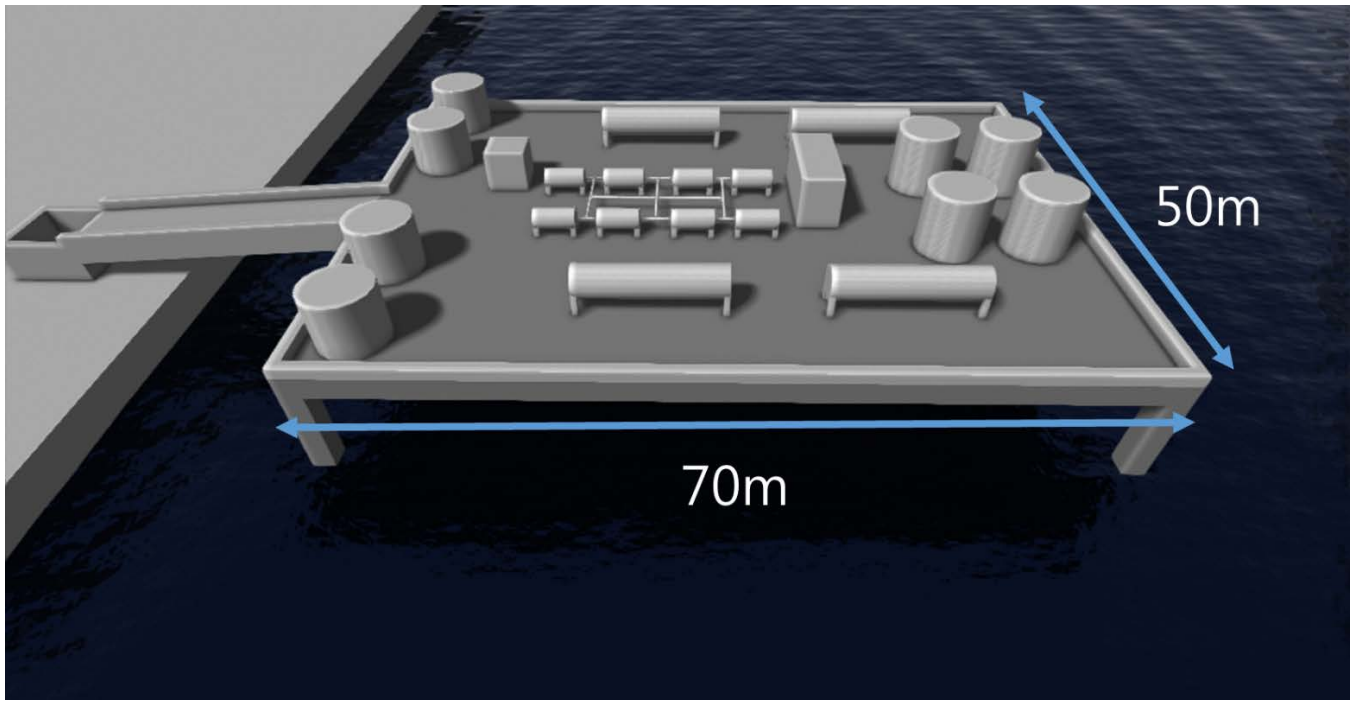

Figure 20 Geometry of an LNG terminal

4.2.3. ANN Regression

Artificial Neural Network calculation is done by Matlab. Size of the hidden layer is a key to proper regression. Too few ANN hidden layer cannot catch the principal tendency, and too many hidden layer would overfit the data. In this paper, 10 hidden layer is used as recommended by Matlab. When using undetected scenario, the quality of the regression is affected by how to set the undetected scenario detection time, so that only detected scenario is used as the regression model. 8 variables, which is 5 input variables in CFD and x, y, z coordinate of the detector location, are used in the input. Figure 22 shows the structure of the constructed neural network.

First, using all the detected scenario data is used to check if the ANN can catch the pattern. And then, all the 30 scenario is tested by LOOCV (Leave-One-Out Cross Validation). LOOCV method is extremely useful when there's not many data sets. Lastly, using all the 47610 data sets including detected and undetected, classification is done to check if undetected scenario affects the quality of the ANN model. After checking ANN by these three kinds of tests, newly created input variables are done. As one of the merits of this surrogate model building is the computation resources, this ANN model takes only several minutes in the personal computer.

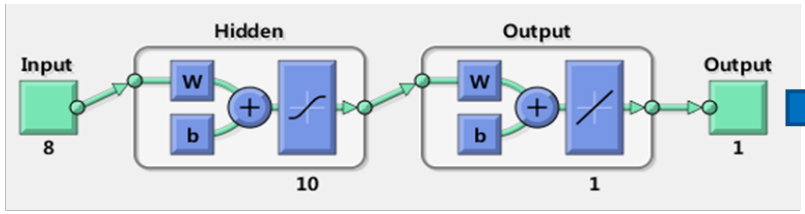

Detection time

Bayesian Regularization back propagation
Based on Levenberg-Marquardt optimization

Meteorological inputs	Leak inputs	Detector location
• Wind speed in x • Wind speed in y	• Mass rate • Location in x • Location in y	• Location in x • Location in y • Location in z

Figure 21 Structure of the ANN

4.2.3. Sensor Allocation

Sensor allocation optimization in this chapter is solved by MILP (Mixed Integer Linear Programming). The problem statement is as below. The formulation of the MILP follows S.W. Legg et al. (2012). The problem notation is summarized in table 9.

$$\min \sum_{a \in A} \alpha_a \sum_{i \in \mathcal{L}_a} d_{a,i} x_{a,i} \qquad \text{(Eq 4-1a)}$$

s.t.

$$\sum_{l \in \mathcal{L}} s_l \leq p \qquad \text{(Eq 4-1b)}$$

$$x_{a,i} \leq s_i \qquad \forall a \in A, \quad i \in \mathcal{L}_a \qquad \text{(Eq 4-1c)}$$

$$\sum_{i \in \mathcal{L}_a} x_{a,i} = 1 \qquad \forall a \in A \qquad \text{(Eq 4-1d)}$$

$$s_l \in \{0, 1\} \qquad \forall l \in L \qquad \text{(Eq 4-1e)}$$

$$0 \leq x_{a,i} \leq 1 \qquad \forall a \in A, \quad i \in \mathcal{L}_a \qquad \text{(Eq 4-1f)}$$

Equation (4-1a) is the objective function to find minimum mean detection time for each scenario a. All scenarios are equally probable in this MILP programming, which is $\alpha_a = 1/M$. The term $d_{a,i}$ is the pre-calculated damage coefficient, it can be defined as expected explosion damage if gas is flammable, or expected toxic damage if the gas is toxic. Here, damage

coefficient is defined as detection time that sensor in i can detect scenario a. The binary variable s_l indicates whether sensor exists ($s_l = 1$) or not ($s_l = 0$). The variable $x_{a,i}$ represents the first existing detector for a scenario. It does not have integer constraint but equation 4-1c, 4-1d, and 4-1f make it have value of 0 or 1. Equation 4-1b restricts maximum number of detectors. Equation 4-1c guarantees existence of the detector when it is the first detector. Equation 4-1d means the first detector is only one, obviously. This MILP gives optimal sensor allocation when given damage coefficient matrix.

Table 9 Problem notation

SYMBOL	MEANING
$\mathbf{L} = \{\mathbf{1}, \mathbf{2}, \mathbf{3}, \dots, \mathbf{N}\}$	Potential detector locations
$\mathbf{A} = \{\mathbf{1}, \mathbf{2}, \mathbf{3}, \dots, \mathbf{M}\}$	Leak scenarios
$\boldsymbol{\mathcal{L}_a}$	Sensor locations affected by scenario a
$\boldsymbol{\alpha_a}$	Probability of leak scenario a
$\boldsymbol{d_{a,i}}$	Damage coefficient for leak scenario a at location i
$\mathbf{p}$	Maximum number of detectors
$\boldsymbol{s_l}$	Binary variable indicating whether a sensor is installed at location l or not
$\boldsymbol{x_{a,i}}$	Indicator for location i that first detects scenario a

4.3. Results

4.3.1. ANN results

After running all the 30 scenarios with 1587 potential detector locations, there are 47610 data sets. As detector location is more likely to be determined by the shorter detector time than longer detection time, log-scaled detection time is more meaningful. Figure 23 is the error histogram between real detection time and estimated detection time, which shows that trained network is well trained without skewness. And most of the data is within the deviation of 0.2, which is about 1.6 times error in the normal scale.

Table 11 below shows LOOCV of all scenarios and MSE (mean squared error) for each scenario. Overall performance based on MSE is 0.0419. Each scenario and predicted value based on the other 29 scenario is well matched with the lowest MSE is 0.0411 and the highest is 0.0652.

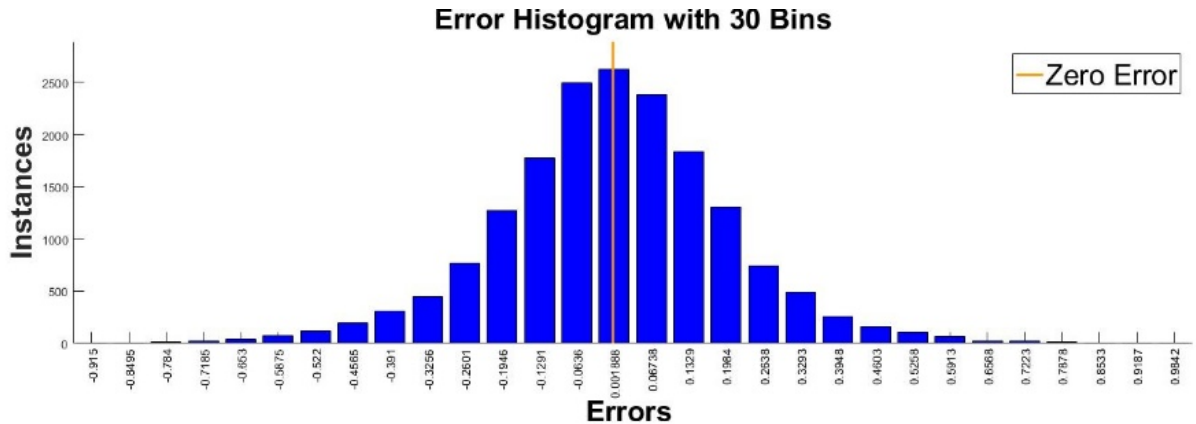

Figure 22 Error histogram of the trained network

Table 10 Cross validation result

Scenario	***Mass***	***Ux***	***Uy***	***Sx***	***Sy***	***MSE***
Unit	**kg/s**	**m/s**	**m/s**	**m**	**m**	
1	11.54	0.43	-1.56	-21.90	-18.94	0.0511
2	10.23	-0.98	-2.64	25.98	8.99	0.0495
3	55.00	0.66	-2.23	27.66	-1.26	0.0450
4	40.85	2.92	1.02	-17.51	-6.19	0.0513
5	38.71	1.40	-2.89	8.33	12.23	0.0453
6	95.45	-1.98	-1.22	4.79	11.48	0.0542
7	46.46	-0.24	3.05	-3.04	19.78	0.0460
8	18.19	-2.44	2.93	-13.89	-14.32	0.0469
9	35.43	-0.50	-0.59	-15.48	13.50	0.0420
10	75.51	-2.23	1.72	-25.40	-9.81	0.0460
11	99.08	3.08	1.48	-9.49	-4.24	0.0446
12	73.74	-0.02	1.30	-19.75	10.67	0.0457
13	26.23	-3.32	0.66	2.07	-7.95	0.0453
14	65.09	-0.76	-1.80	12.04	-2.87	0.0489
15	78.09	3.42	-0.45	-23.84	-17.24	0.0587
16	50.33	-1.50	-0.09	15.43	3.43	0.0460
17	32.76	2.54	2.18	23.88	6.37	0.0483
18	16.09	1.07	-3.47	16.36	-10.85	0.0411
19	43.66	-2.96	-2.45	1.64	-8.35	0.0411
20	22.80	0.81	3.35	11.93	7.27	0.0556
21	89.81	-1.25	2.46	-5.54	17.22	0.0407
22	28.04	1.95	0.21	-7.08	4.54	0.0425
23	91.22	2.17	0.91	-28.66	-17.37	0.0652
24	56.64	0.20	2.07	20.84	-1.94	0.0453
25	60.04	-2.67	-1.97	-27.71	2.22	0.0443
26	84.92	-3.25	0.25	-1.28	0.08	0.0440
27	82.55	-1.77	-3.18	-10.84	-11.07	0.0447
28	70.46	1.50	-0.92	6.91	-12.57	0.0411
29	8.16	2.62	-0.95	29.64	17.79	0.0434
30	66.49	1.81	2.73	19.53	10.16	0.0445

4.3.2. Sensor Allocation Result

The MILP has to decide existence of the detector at the potential detector location, s_l, which is an integer variable and the number is 1587. There is massive number of coefficients in constraints especially in the inequality constraints. As Matlab cannot handle the coefficient matrix directly, a sparse coefficient matrix was used.

Figure 24 shows detector allocation optimization result. It has both result of basic 30 scenarios and extended 130 scenarios. When using 30 scenario, the more detector the less detection time to converge to minimum detection time of 5 second, which is start of the leak and it means that sensor can detect the any leak almost immediately. When extended scenario is used, the tendency is similar but it does not go to the minimum detection point because the detectors cannot cover the leak one-by-one. Still, it is better to have good coverage for non-simulated scenarios.

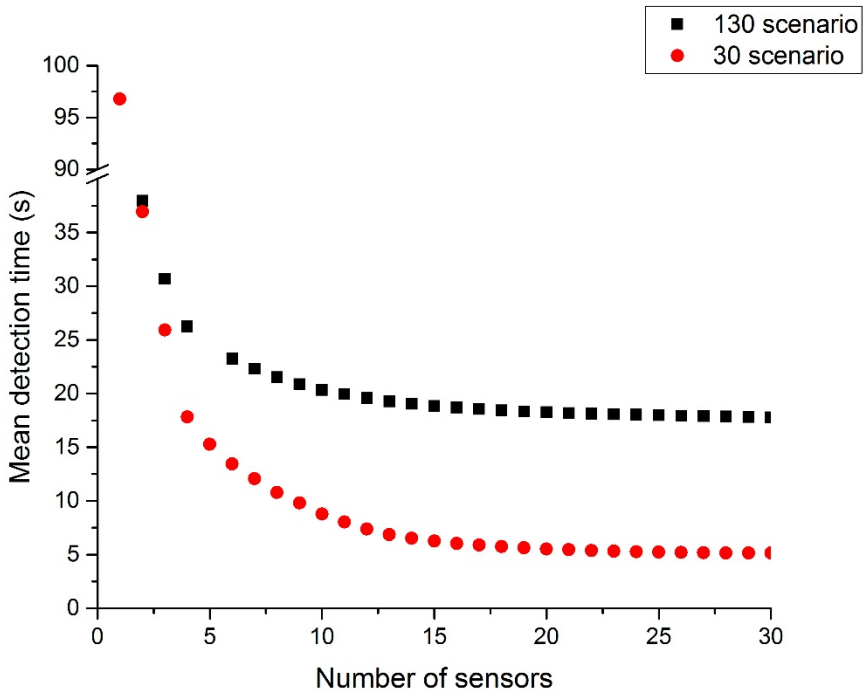

Figure 23 Detection time by number of sensors

4.3.3. Discussion

To prove this meta-model based optimization is practical, two things should be discussed. First, as undetected data sets are not included in the regression, some tests needs to be done including the undetected dataset. Although it might have some distribution to estimate actual detection time, the chance of misclassification whether the detector actually detect or not within some time before some time near mean detection time is low. For the classification problem 30s was used. Number of the hidden layer is 10 as same as the regression problem. Scaled conjugate gradient training method is used and training performance is calculated with cross entropy term. Training set is 70%, validation 15%, and testing 15%. Table 11 shows the results. Almost every scenario can be classified into detected and undetected within 30s. So even after including the undetected scenario, the ANN training is well-defined.

Second question is that the extended scenario can cover the entire process layer. Figure 25 and 26 shows that when 130 scenario is used, the detectors are away from the simulated source directly unlikely the 30 scenario case.

Table 11 Confusion matrix of trained network

		Target Class		Overall Accuracy
		Not Detect (0)	Detect (1)	
Output Class	Not Detect (0)	True Negative 44141 (92.7%)	False Negative 27 (0.1%)	99.9%
	Detect (1)	False Positive 19 (0.0%)	True Positive 3423 (7.2%)	99.4%
Overall Accuracy		100.0%	99.2%	99.9%

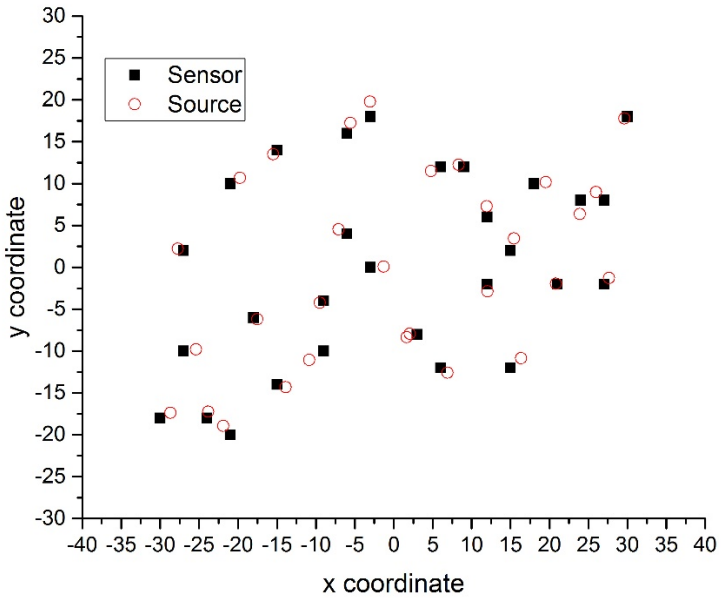

Figure 24 30 scenarios, 30 detectors

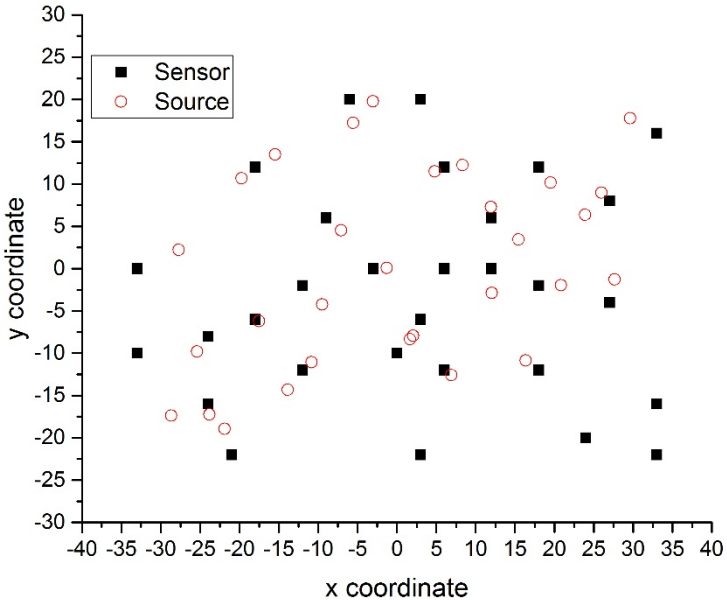

Figure 25 130 scenarios, 30 detectors

4.4. Chapter conclusion

In this chapter, application of the surrogate model technology for the detector allocation optimization problem is dealt. It would help CFD to become useful and affordable technology in the field of chemical safety, which needs a lot of simulation. Real-time dispersion prediction and QRA (Quantitative Risk Analysis) would be promising future work when combined with model reduction technics such as POD. And the development of detector optimization techniques especially imperfect detector allocation optimization is applicable in the future.

Chapter 5: Conclusion

5.1. Concluding remarks

This thesis can be summarized as below.

First, CFD simulation is useful and valid when modeling hazardous chemical dispersion in the atmosphere. CFD shows good match with the experimental dispersion data and its prediction accords with the actual accidental consequences.

Second, CFD simulation can model the more complex geometry such as urban area and the simulation time can be reduced with time variant numerical stepping and multithreading, and even shows the possibility of real-time modeling with the help of ANN technology.

Third, CFD simulation can be used in the optimization programming with the help of surrogate modeling. Together with ANN, CFD model overcomes the computational burden and can give the data basis for the optimization.

5.2. Future works

For the future works, some chemical process safety application such as real-time dispersion prediction, or it might be able to predict the explosion damage or fire intensity. Based on these prediction QRA can be conducted three-dimensionally without having to take so much time modeling in CFD. This thesis didn’t include the model reduction but for analysis in three dimension with time varying data, reduction techniques such as PCA should be considered.

Nomenclature

Variables are in the main text

▶ Abbreviation

ANN: Artificial Neural Network

CAD: Computer Aided Design

CFD: Computational Fluid Dynamics.

CFL: courant-Friedrich-Levy number

DACE: Design and Analysis of Computer Experiment

DoE: Design of Experiment

ERPG: Emergency Response Planning Guideline

FLACS: Flame Acceleration Simulator

GF: Gold Fish

HEM: Homogeneous Equilibrium Model

HF: Hydrogen Fluoride

KST: Korean Standard Time

LCD: Liquid Crystal Display

LES: Large Eddy Simulation

LFL: Lower Flammability Limit

LHS: Latin Hypercube Sampling

LNG: Liquefied Natural Gas

LOOCV: Leave one out cross validation

MILP: Mixed Integer Linear Programming

MRB: Mean Relative Bias

MRSE: Mean Relative Square Error

NSIC: National Spatial Information Clearinghouse

PCA: Principal Component Analysis

POD: Proper Orthogonal Decomposition

QRA: Quantitative Risk Analysis

RANS: Reynolds Averaged Navier Stokes

ROC: Relative Operating Curve

Literature cited

▶ Chapter 1

FLACS User Manual, 2015

Blewitt, D. N., J. F. Yohn, R. P. Koopman and T. C. Brown (1987). Conduct of Anhydrous Hydrofluric Acid Spill Experiment, Lawrence Livermore National Laboratory.

Dogeroglu, T., A. Cicek and S. Kara (2003). "Short-term effects of hydrogen fluoride on Nicotiana tabacum L." J Environ Sci Health B 38(5): 561-570.

Gexcon AS. (2015). FLACS v10.4 User's Manual.

Gu, S., I. Choi, W. Kim, O. Sun, S. Kim and Y. Lee (2013). "Study on the Distribution of Fluorides in Plants and the Estimation of Ambient Concentration of Hydrogen Fluoride Around the Area of the Accidental Release of Hydrogen Fluoride in Gumi." Korean Journal of Environmental Health Sciences 39(4): 346-353.

Hanna, S. R., O. R. Hansen and S. Dharmavaram (2004). "FLACS CFD air quality model performance evaluation with Kit Fox, MUST, Prairie Grass, and EMU observations." Atmospheric Environment 38(28): 4675-4687. DOI:10.1016/j.atmosenv.2004.05.041

Hanna, S. R., D. G. Strimaitis and J. C. Chang (1991). "Evaluation of fourteen hazardous gas models with ammonia and hydrogen fluoride field data." Journal of Hazardous Materials 26: 127-158.

Hansen, O. R., F. Gavelli, M. Ichard and S. G. Davis (2010).

"Validation of FLACS against experimental data sets from the model evaluation database for LNG vapor dispersion." Journal of Loss Prevention in the Process Industries 23(6): 857-877. DOI: 10.1016/j.jlp.2010.08.005

Horntvedt, R. (1997). "Accumulation of airborne fluorides in forest trees and vegetation." European Journal of Forest Pathology 27(2): 73-82. DOI: 10.1111/j.1439-0329.1997.tb01358.x

Hyun, C. U., J. S. Lee and I. Lee (2013). "Assessment of hydrogen fluoride damage to vegetation using optical remote sensing data." ISPRS - International Archives of the Photogrammetry, Remote Sensing and Spatial Information Sciences XL-7/W2: 115-118. DOI:10.5194/isprsarchives-XL-7-W2-115-2013

Ichard, M. (2012). Numerical computations of pressurized liquefied gas releases into the atmosphere. PhD, University of Bergen.

Ivings, M. J., C. J. Lea, D. M. Webber, S. F. Jagger and S. Coldrick (2013). "A protocol for the evaluation of LNG vapour dispersion models." Journal of Loss Prevention in the Process Industries 26(1): 153-163. DOI: 10.1016/j.jlp.2012.10.005

Joo, H. S. (2013). A study on the improvement of environmental impact assessment of industrial complexes based on risk assessment of chemical leakeage accidents. K. E. Institute.

Ko, M. W., C. B. Oh, Y. S. Han, B. I. Choi, K. H. Do, M. B. Kim and T. H. Kim (2015). "Large Eddy Simulation for the Prediction of Unsteady Dispersion Behavior of Hydrogen Fluoride." Journal of the Korean Society of Safety 30(1): 14-20. DOI : 10.14346/JKOSOS.2015.30.1.014

Koh, D. H. (2014). A study on the establishment of environmental impact area of hydrofluoric acid spill in Gumi, Korea, Seoul National University.

Korea Occupational Safety & Health Agency (2013). Case study of hydrogen fluoride accidental release (in Korean).

Kwanghee Lee, Hyuk-myun Kwon, Seugsik Cho, Jiyong Kim, Il Moon (2016). "Improvement of safety after a large chemical accident" Journal of Loss Prevention in Process Industries 42 6-13.

Kwon, E., H. A. Lee, D. Kim, J. Lee, S. Lee and H.-O. Yoon (2015). "Geochemical Investigation of Fluoride Migration in the Soil Affected by an Accidental Hydrofluoric Acid Leakage." Journal of Soil and Groundwater Environment 20(3): 65-73.

L.H.Weinstein and A.W.Davison (2004). Fluorides in the Environment, CABI Publishing.

Lee, M.-R., S. Koo and J.-H. Shim (2013). "Assessment of Estimated Damage Area by CCTV Images: Case Study of Gumi Hydrofluoric Acid Gas Leakage." Journal of Korean Society of Hazard Mitigation 13(6): 223-229.

Lophaven, S. N., H. B. Nielsen and J. Søndergaard (2002). DACE A MATLAB Kriging Toolbox, Technical University of Denmark.

MacLean, D. C., D. C. McCune, L. H. Weinstein, R. H. Mandl and G. N. Woodruff (1968). "Effects of acute hydrogen fluoride and nitrogen dioxide exposures on citrus and ornamental plants of central Florida." Environmental Science & Technology 2(6): 444-449. DOI: 10.14288/1.0088083

Weinstein, L. H. and A. W. Davison (2003). "Native plant species suitable as bioindicators and biomonitors for airborne fluoride." Environmental Pollution 125(1): 3-11. DOI: 10.1016/S0269-7491(03)00090-3

Yang, S., J. Jeon, Y. Lee, G. Lee and C. Han (2015). "Study on Estimation of Ambient Hydrogen Fluoride Concentration of Accident Release Simulation based on Dry Deposition on Vegetation." Korean Journal of Hazardous Materials 3(1): 1-6.

Yang S., J. Jeon, D. Kang, C. Han (2017). “Accident analysis of Gumi hydrogen fluoride gas leak using CFD and comparison with post-accidental environmental impacts” Journal of Loss Prevention in the Process Industries 48, 207-215

Yim, B. and S.-T. Kim (2016). "Estimation of the Concentration of HF in the Atmosphere Using Plant Leaves Exposed to HF in the Site of the HF Spill." Journal of Korean Society for Atmospheric Environment 32(3): 248-255. DOI : 10.5572/KOSAE.2016.32.3.248

▶ Chapter 3

Zhang, B.; Chen, G.-m., Quantitative risk analysis of toxic gas release caused poisoning—A CFD and dose–response model combined approach. Process Safety and Environmental Protection 2010, 88 (4), 253-262.

Dharmavaram, S.; Hanna, S. R.; Hansen, O. R., Consequence analysis—Using a CFD model for industrial sites. Process Safety Progress 2005, 24 (4), 316-272.

Mazzoldi, A.; Hill, T.; Colls, J. J., Assessing the risk for CO2

transportation within CCS projects, CFD modelling. International Journal of Greenhouse Gas Control 2011, 5 (4), 816-825.

Siddiqui, M.; Jayanti, S.; Swaminathan, T., CFD analysis of dense gas dispersion in indoor environment for risk assessment and risk mitigation. J Hazard Mater 2012, 209-210, 177-85.

Tominaga, Y.; Stathopoulos, T., CFD simulation of near-field pollutant dispersion in the urban environment: A review of current modeling techniques. Atmospheric Environment 2013, 79, 716-730.

Hanna, S. R.; Hansen, O. R.; Ichard, M.; Strimaitis, D., CFD model simulation of dispersion from chlorine railcar releases in industrial and urban areas. Atmospheric Environment 2009, 43 (2), 262-270.

Sanchez, E. Y.; Colman Lerner, J. E.; Porta, A.; Jacovkis, P. M., Accidental release of chlorine in Chicago: Coupling of an exposure model with a Computational Fluid Dynamics model. Atmospheric Environment 2013, 64, 47-55.

Xie, Z.-T.; Castro, I. P., Large-eddy simulation for flow and dispersion in urban streets. Atmospheric Environment 2009, 43 (13), 2174-2185.

Lateb, M.; Masson, C.; Stathopoulos, T.; Bédard, C., Effect of stack height and exhaust velocity on pollutant dispersion in the wake of a building. Atmospheric Environment 2011, 45 (29), 5150-5163.

Hanna, S. R.; Brown, M. J.; Camelli, F. E.; Chan, S. T.; Coirier, W. J.; Kim, S.; Hansen, O. R.; Huber, A. H.; Reynolds, R. M., Detailed Simulations of Atmospheric Flow and Dispersion in Downtown Manhattan: An Application

of Five Computational Fluid Dynamics Models. Bulletin of the American Meteorological Society 2006, 87 (12), 1713-1726.

Gexcon AS, FLACS v10.4 User's Manual, July 2015.

BH Hjertager; Computer simulation of turbulent reactive gas dynamics. Modeling, Identification and Control, 1984, 5 (4), 211-236

H. M. Bücker; B. Pullul; A. Rasch, On CFL evolution strategies for implicit upwind methods in linearized Euler equations, International Journal for Numerical Methods in Fluids, 2009 59, 1-18

Chenzhou Lian; Guoping Xia; Charles L. Merkle, Solution-limited time stepping to enhance reliability in CFD applications, Journal of Computational Physics, 2009, 228(13), 4836-4857

Center for Chemical Process Safety of the American Institute of Chemical Engineers, Guidelines for Chemical Process Quantitative Risk Analysis, 2000, second edition,, 590p { Originally from Withers, R. M. J.; F. P. Lees, The Assessment of Major Hazards: The Lethal Toxicity of Chlorine, Parts 1 and 2, Journal of Hazardous Materials, 1985, 12 (3) }

Korean Industrial Complex Corp., Ulsan-Mipo National Industrial Complex, 2013, [http://www.e-cluster.net]

National Spatial Information Clearinghouse (NSIC). [https://www.nsic.go.kr] (Cannot access outside of Republic of Korea)

Google Earth Image [https://www.google.com/earth/]

Spatial Information Industry Promotion Institute, [http://vwold.kr]

▶ Chapter 4

Benavides-Serrano, A. J., S. W. Legg, R. Vázquez-Román, M. S. Mannan and C. D. Laird (2014). “A Stochastic Programming Approach for the Optimal Placement of Gas Detectors: Unavailability and Voting Strategies.” Industrial & Engineering Chemistry Research 53: 5355-5365.

Benavides-Serrano, A. J., M. S. Mannnan and C. D. Laird (2015). “A quantitative assessment on the placement practices of gas detectors in the process industries.” Journal of Loss Prevention in the Process Industries 35: 339-351.

Benavides-Serrano, A. J., M. S. Mannnan and C. D. Laird (2016). “Optimal Placement of Gas Detectors: A P-Median Formulation Considering Dynamic Nonuniform Unavailabilities.” American Institute of Chemical Engineers 62(8): 2728-2739

Berry, J., W. E. Hart, C. A. Phillips and J. Uber (2004). “General Integer-Programming-Based Framework for Sensor Placement in Municipal Water Networks.” World Water Congress 2004.

Berry, J., W. E. Hart, C. A. Phillips, J. G. Uber and J. Watson (2006). “Sensor Placement in Municipal Water Networks with Temporal Integer Programming Models.” Journal of Water Resources Planning and Management 132(4): 218-224.

Berry, J., R. D. Carr, W. E. Hart, V. J. Leung, C. A. Phillips and J. Watson (2006). “ON THE PLACEMENT OF IMPERFECT SENSORS IN MUNICIPALWATER NETWORKS.” Water Distribution Systems Analysis Symposium 2006.

Bezzo, F., S. Macchietto and C. C. Pantelides (2000). “A general

framework for the integration of computational fluid dynamics and process simulation.” Computers and Chemical Engineering 24:653-658.

Cai, H., X. Li, Z. Chen and L. Kong (2013). “Fast Identification of Multiple Indoor Constant Contaminant Sources by Ideal Sensors: A Theoretical Model and Numerical Validation.” Indoor and Built Environment 22(6):897-909.

Davis, S., O. R. Hansen, F. Gavelli and A. Bratteteig (2011). Using CFD to analyze gas detector placement in process facilities. Mary Kay O'Connor Process Safety Center Sysmposium 2011. College Station, Texas, USA. International Process Safety Symposium 2011.

Defriend, S., M. Dejmek, L. Porter, B. Deshotels and B. Natvig (2008). "A risk-based approach to flammable gas detector spacing." J Hazard Mater 159(1): 142-151.

Hamel, D., M. Chwastek, B. Farouk, K. Danderkar and M. Kam (2006). A Computational Fluid Dynamics Approach for Optimization of a Sensor Network. IEEE International Workshop on Measurement Systems for Homeland Security. Alexandria, VA, USA.

Hansen, O. R., F. Gavelli, M. Ichard and S. G. Davis (2010). "Validation of FLACS against experimental data sets from the model evaluation database for LNG vapor dispersion." Journal of Loss Prevention in the Process Industries 23(6): 857-877.

Legg, S. W., A. J. Benavides-Serrano, J. D. Siirola, J. P. Watson, S. G. Davis, A. Bratteteig and C. D. Laird (2012). "A stochastic programming approach for gas detector placement using CFD-based dispersion simulations."

Computers & Chemical Engineering 47: 194-201.

Legg, S. W., C. Wang, A. J. Benavides-Serrano and C. D. Laird (2013). "Optimal gas detector placement under uncertainty considering Conditional-Value-at-Risk." Journal of Loss Prevention in the Process Industries 26(3): 410-417.

Margheri, L. and P. Sagaut (2016). “A hybrid anchored-ANOVA – POD/Kriging method for uncertainty quantification in unsteady high-fidelity CFD simulations.” Journal of Computational Physics 324: 137-173.

Rad, A., D. Rashtchian and N. Badri (2017). “A risk-based methodology for optimum placement of flammable gas detectors within open process plants.” Process Safety and Environmental Protection 105: 175-183.

Shyla, M. V., K. B. Naldu and G. V. Kumar (2013). “Optimization of Sensor Position on Different Surfaces Using CFD Analysis for Reducing Accidents Caused by Emission of Toxic Gas in Industries.” 2013 Fifth International Conference on Advanced Computing.

Shyla, M. V., K. B. Naldu and G. V. Kumar (2014). “Fixing Sensor Position Using Computational Fluid Dynamic Analysis for Trace Detection of Toxic Gases.” Indian Journal of Science and Technology 7(12): 1987-1998.

Stoecklein, D., K. G. Lore, M. Davies, S. Sarkar and B. Ganapathysubramanian (2017). “Deep Learning for Flow Sculpting: Insights into Efficient Learning using Scientific Simulation Data.” Scientific Reports 7:46368.

Vázquez-Román, R., C. Díaz-Ovalle, E. Quiroz-Pérez and M. S. Mannan (2016). "A CFD-based approach for gas detectors allocation." Journal

of Loss Prevention in the Process Industries 44: 633-641.

Vianna, Sávio S. V., Juliane Fiates, Vinicius Simoes (2015) “OPTIMI – A Novel 3D Computational Tool for Gas Detector Optimisation.”

Worden, K. and A. P. Burrows (2001). “Optimal sensor placement for fault detection.” Engineering Structures 23: 885-901.

Abstract in Korean (요 약)

유해화학물질 확산 분석 및 인공신경망을 사용한 대리 모델 최적화

전산유체역학 모사는 유해화학물질로 인한 사고의 피해 결과를 추정하는데 사용할 수 있다. 이 모사의 장점과 단점은 모두 전산유체역학의 복잡성과 관련되어 있다. 전산유체역학은 도시 지역과 같이 복잡한 지형에서의 화학물질 확산 현상을 예측할 수 있지만 계산 자원이 많이 필요하다는 단점이 있다.

이러한 전산유체역학 모사의 유용성을 보여주기 위하여 실제 확산 결과와 전산유체역학 모사간의 비교가 수행되었다. 무수 불화수소 확산 현장시험 결과는 모사 결과 확산모델 사용기준을 만족하였다. 2012년의 실제 불화수소 누출 사고도 모사 결과 역시 사람과 환경에 대한 피해가 실제와 유사했다.

도시지역에서 누출원 및 기상 조건에 다른 독성 가스 확산 케이스 스터디가 수행되었으며 최악의 시나리오에 대해서는 수치적 방법을 테스트했다. 시간에 따른 CFL 증가 및 다중 스레드 기법이 사용되어 시뮬레이션에 필요한 시간을 줄일 수 있었다. 인공신경망을 사용하여 안전지역 및 위험지역을 분류하는 것도 가능했다.

전산유체역학 모사는 공정에서 감지기 배치 문제에도 적용될 수

있다. 모사 입력조건은 컴퓨터 실험 절차에 따라 결정되었고 다른 데이터 세트의 감지시간은 인공신경망으로 추정되었다. 이 모사 결과 및 추정 결과를 사용하여 정수혼합 선형최적화 결과는 모사 결과만을 사용할 때보다 더 좋은 결과를 보였다.

주요어: 전산유체역학, 화학물질 안전, 인공신경망, 정수혼합 선형최적화, 대리모델

학번: 2011-21045

성명: 양 시 엽

Hazardous Chemical Dispersion Analysis and Surrogate Model Optimization using Artificial Neural Network

유해화학물질 확산 분석 및 인공신경망을 사용한 대리 모델 최적화

지도교수 한 종 훈

이 논문을 공학박사학위논문으로 제출함

2017 년 5 월

서울대학교 대학원

화학생물공학부

양 시 엽

양시엽의 박사학위논문을 인준함

2017 년 7 월

위 원 장 이 원 보 (인)

부 위 원 장 한 종 훈 (인)

위 원 尹 宣 燮 (인)

위 원 임 영 섭 (인)

위 원 이 철 진 (인)